Department of Applied Physics

Magnetization dynamics and energy dissipation in magnetic thin films

Ilari Rissanen

Aalto University

DOCTORAL DISSERTATIONS

Supervising professor
Prof. Mikko Alava, Aalto University, Finland

Thesis advisor
Assoc. Prof. Lasse Laurson, Tampere University, Finland

Preliminary examiners
Dr. Andrea Vanossi, CNR-IOM DEMOCRITOS Simulation Center
& International School for Advanced Studies (SISSA), Italy
Dr. Jonathan Leliaert, Ghent University, Belgium

Opponent
Prof. Hans-Josef Hug, University of Basel, Switzerland

Aalto University publication series
DOCTORAL DISSERTATIONS 161/2019

ISBN 978-952-60-8705-4 (printed)
ISBN 978-952-60-8706-1 (pdf)
ISSN 1799-4934 (printed)
ISSN 1799-4942 (pdf)
http://urn.fi/URN:ISBN:978-952-60-8706-1

Unigrafia Oy
Helsinki 2019

Finland

NORDIC SWAN ECOLABEL
Printed matter
4041-0619

Aalto University

Abstract

Aalto University, P.O. Box 11000, FI-00076 Aalto www.aalto.fi

Author
Ilari Rissanen

Name of the doctoral dissertation
Magnetization dynamics and energy dissipation in magnetic thin films

Publisher School of Science

Unit Department of Applied Physics

Series Aalto University publication series DOCTORAL DISSERTATIONS 161/2019

Field of research Theoretical and Computational Physics

Manuscript submitted 17 June 2019 **Date of the defence** 10 October 2019

Permission for public defence granted (date) 22 August 2019 **Language** English

☐ **Monograph** ☒ **Article dissertation** ☐ **Essay dissertation**

Abstract

Magnetic thin films are layers of magnetic material ranging from ultrathin films, consisting of only a few atomic layers, up to few micrometers in thickness. The magnetization configurations of magnetic thin films display a wide variety of complex patterns, including bubbles domains, maze patterns and topological solitons or defects. Under the influence of e.g. external magnetic field, the magnetization exhibits rich dynamics, from avalanche-like domain wall jumps in Barkhausen noise to nucleation and annihilation of vortices and antivortices in in-plane anisotropy films. Magnetic thin films are researched extensively due to their unique properties and potential for nano- and microscale applications, such as magnetic memory devices and microelectromechanical systems (MEMS).

When the magnetization of a magnet goes through a change due to e.g. domain wall motion in the aforementioned Barkhausen noise, the elementary magnetic moments of the system experience motion called Larmor precession, which slowly winds down as the magnetization relaxes into a new configuration. This relaxation results from couplings between magnetic, electric and phononic degrees of freedom, which transfer energy from the magnetic moments to the lattice, where the energy is then dissipated as heat. These magnetic losses are relevant in applications where there are alternating electromagnetic fields or components moving in such fields, such as transformers, electric motors and magnetic bearings.

In this dissertation, we study magnetic losses in thin films using micromagnetic simulations, with emphasis on the magnetization dynamics and dissipation resulting from the motion of a magnetic thin film in an external field or relative to another film. Publication I focuses on the dynamics of topological defects and energy dissipation in a Permalloy thin film experiencing a relaxation from an initially random magnetization state. In publication II, we develop an extension capable of simulating moving thin films to an existing micromagnetic simulation code. Publications III and IV use the extension to investigate domain wall dynamics and the resulting losses in response to motion in thin films with perpendicular magnetic anisotropy. Publication III investigates the damping of high-frequency mechanical oscillation due to magnetic dynamics, while publication IV considers magnetic losses due to domain wall motion in films with disorder.

Keywords micromagnetics, domain dynamics, magnetic friction, simulations

ISBN (printed) 978-952-60-8705-4 **ISBN (pdf)** 978-952-60-8706-1

ISSN (printed) 1799-4934 **ISSN (pdf)** 1799-4942

Location of publisher Helsinki **Location of printing** Helsinki **Year** 2019

Pages 106 **urn** http://urn.fi/URN:ISBN:978-952-60-8706-1

Tekijä
Ilari Rissanen

Väitöskirjan nimi
Magnetisaation dynamiikka ja energiahäviöt magneettisissa ohutkalvoissa

Julkaisija Perustieteiden korkeakoulu

Yksikkö Teknillisen fysiikan laitos

Sarja Aalto University publication series DOCTORAL DISSERTATIONS 161/2019

Tutkimusala Teoreettinen ja laskennallinen fysiikka

Käsikirjoituksen pvm 17.06.2019 **Väitöspäivä** 10.10.2019

Väittelyluvan myöntämispäivä 22.08.2019 **Kieli** Englanti

☐ **Monografia** ☒ **Artikkeliväitöskirja** ☐ **Esseeväitöskirja**

Tiivistelmä

Magneettiset ohutkalvot ovat magneettisesta materiaalista valmistettuja kerroksia, joiden paksuus vaihtelee kalvosta riippuen muutamasta atomikerroksesta (ns. ultraohut kalvo) muutamaan mikrometriin. Magneettisissa ohutkalvoissa esiintyy monipuolisia magnetisaatiorakenteita, kuten magneettisia kuplia, sokkelomaisia kuvioita ja topologisia solitoneja tai defektejä. Magnetisaation dynamiikka, joka voidaan saada aikaan esimerkiksi ulkoista magneettikenttää käyttäen, on magneettisissa ohutkalvoissa hyvin monimuotoista, sisältäen muun muassa magneettisten seinämien vyörymäisiä liikkeitä (niin kutsuttua Barkhausenin kohinaa) sekä vorteksien ja antivorteksien synty- ja annihilaatioprosesseja tasoon magnetoituneissa ohutkalvoissa. Magneettisia ohutkalvoja tutkitaan paljon niiden erityisten magneettisten ominaisuuksien sekä potentiaalisten sovellusten, kuten magneettisten muistien ja mikroelektromekaanisten systeemien (MEMS) vuoksi.

Magnetisaation muutos, esimerkiksi magneettisen seinämän liikkuessa edellämainitussa Barkhausenin kohinassa, saa materiaalin alkeismagneeteissa aikaan pyörimisliikkeen, joka tunnetaan Larmorin prekessiona. Tämä prekessioliike vaimenee nopeasti, ja magnetisaatio mukautuu uuteen konfiguraatioon. Liikkeen vaimeneminen johtuu kytkennöistä aineen magneettisten, sähköisten ja fononisten vapausasteiden välillä, jotka muuntavat magneettisten momenttien liikeenergiaa hilarakenteen lämpövärähtelyiksi. Tämänkaltaiset magneettiset häviöt ovat oleellisia sovelluksissa, joissa on muuttuvia sähkömagneettisia kenttiä tai liikkuvia komponentteja sähkömagneettisissa kentissä, kuten muuntajissa, sähkömoottoreissa ja magneettisissa laakereissa.

Tässä työssä tutkitaan magneettisia häviöitä ohutkalvoissa mikromagnetismisimulaatioiden avulla. Tutkimuksen painopisteenä ovat magnetisaation dynamiikka ja häviöt, jotka johtuvat ohutkalvon liikkeestä joko ulkoisessa kentässä tai suhteessa toiseen ohutkalvoon. Julkaisu I keskittyy topologisten defektien dynamiikkaan ja energiahäviöihin Permalloy-ohutkalvossa, joka relaksoituu satunnaisesta magneettisesta konfiguraatiosta. Julkaisussa II kehitämme olemassaolevaan mikromagnetismisimulaatio-ohjelmistoon laajennuksen, jolla voimme tutkia liikkuvia ohutkalvoja. Julkaisut III ja IV käyttävät laajennusta magneettisten seinämien dynamiikan ja siitä johtuvien häviöiden tutkimiseen kohtisuoran magneettisen anisotropian ohutkalvoissa. Julkaisussa III syvennytään magnetisaatiodynamiikan aiheuttamaan korkeataajuisen mekaanisen oskillaation vaimenemiseen, ja julkaisussa IV keskitytään magneettisiin häviöihin, jotka johtuvat magneettisten seinämien liikkeestä epäjärjestystä sisältävissä ohutkalvoissa.

Avainsanat mikromagnetismi, domain-dynamiikka, magneettinen kitka, simulointi

ISBN (painettu) 978-952-60-8705-4 **ISBN (pdf)** 978-952-60-8706-1

ISSN (painettu) 1799-4934 **ISSN (pdf)** 1799-4942

Julkaisupaikka Helsinki **Painopaikka** Helsinki **Vuosi** 2019

Sivumäärä 106 **urn** http://urn.fi/URN:ISBN:978-952-60-8706-1

Preface

First of all, I'd like to express my heartfelt gratitude to my supervisor, Prof. Mikko Alava, and thesis advisor, Assoc. Prof. Lasse Laurson, for giving me the opportunity to do write my dissertation in the CSM group and the academic guidance along the way.

I also gratefully acknowledge the Science-IT and CSC computing clusters as the backbone of the simulations of this dissertation, without the considerable computing power of the Triton and Taito clusters and the diligence of the staff maintaining them, this work wouldn't have been possible.

Last but not least, I'd like to thank my friends (particularly those at #e_e) and family for their unending support and encouragement. Working on the dissertation was not always effortless, it is thanks to you that I managed to persevere to the end.

Helsinki, August 28, 2019,

Ilari Rissanen

Contents

List of Publications

This thesis consists of an overview and of the following publications which are referred to in the text by their Roman numerals.

I I. Rissanen & L. Laurson. Coarsening dynamics of topological defects in thin permalloy films. *Physical Review B*, 94, 144428, October 2016.

II I. Rissanen & L. Laurson. Moving magnets in a micromagnetic finite difference framework. *Physical Review E*, 97, 053301, May 2018.

III I. Rissanen & L. Laurson. Magnetic non-contact friction from domain wall dynamics actuated by oscillatory mechanical motion. *Journal of Physics D: Applied Physics*, 52, 445002, August 2019.

IV I. Rissanen & L. Laurson. Bursty magnetic friction between polycrystalline thin films with domain walls. Submitted to *Physical Review B*, June 2019.

Author's Contribution

Publication I: "Coarsening dynamics of topological defects in thin permalloy films"

The author implemented the method for topological defect tracking, performed the simulations, analyzed the results, prepared the figures and wrote the main body of the text, excluding the introduction.

Publication II: "Moving magnets in a micromagnetic finite difference framework"

The author implemented the methods detailed in the article, performed the simulations, analyzed the results, prepared the figures and wrote the majority of the text.

Publication III: "Magnetic non-contact friction from domain wall dynamics actuated by oscillatory mechanical motion"

The author performed the simulations, analyzed the results, prepared the figures and wrote most of the text.

Publication IV: "Bursty magnetic friction between polycrystalline thin films with domain walls"

The author performed the simulations, analyzed the results, prepared the figures and wrote most of the text.

1. Introduction

This dissertation belongs to the field of computational physics and micromagnetism, concentrating on the energy losses related to the magnetization dynamics in ferromagnetic thin films, investigated through numerical micromagnetic simulations. The main subject of the dissertation is thin films in motion under an applied magnetic field or relative to another film, such that the magnetization dynamics are triggered by the motion and the resulting energy dissipation due to magnetic relaxation is interpreted as a source of magnetic non-contact friction. The dissertation is compiled from peer reviewed journal articles, included at the end of the dissertation. The following chapters provide an introduction to the subject matter, while the publications themselves contain the exact details of the methods and results.

1.1 Ferromagnetism

Ferromagnetic materials are those which are commonly referred to as just ”magnetic materials”, possessing the features conventionally associated with magnetism, such as the ability to attract and magnetize other magnetic substances [1]. Though all substances are magnetic to an extent, diamagnetic, paramagnetic and antiferromagnetic materials are typically referred to as non-magnetic, due to the magnetization of these materials requiring sensitive laboratory equipment to measure, and the fact that they demagnetize rapidly after the magnetizing influence, e.g. an externally applied field, is turned off. By contrast, ferromagnetic materials become magnetized easily, and when a field is applied and then removed, the magnetization does not return to its original value, a phenomenon known as hysteresis [2]. Throughout history, ferromagnetic materials have served a purpose in many important applications, ranging from compasses to modern devices essential to everyday life, e.g. electric motors and generators, transformers and recording heads in hard disk drives.

The source of magnetism lies at the atomic level: the magnetic dipole

moments observed in bulk matter arise from the motion of electrons about their atomic nucleus (orbital angular momentum) and the rotation of the electron about its own axis (spin angular momentum) [3]. The nucleus itself also has a magnetic moment, but it is typically negligible compared to the electron magnetic moment. In ferromagnetic materials, the individual magnetic moments have a strong tendency to align in parallel, a phenomenon first explained by the molecular field theory by Weiss in 1906, and later made more accurate by Heisenberg by introducing exchange forces arising from the quantum-mechanical exchange interaction [4]. When heated to a certain temperature called the Curie point, which depends on the material, a ferromagnet loses its magnetization and becomes paramagnetic. The loss of magnetization above Curie temperature is due to the thermal excitations overcoming the exchange interaction, resulting in the breakdown of long range order and thus the vanishing of the net magnetic moment.

In nanoscale ferromagnets, the exchange interaction can be strong enough to force a uniform magnetization across the magnet. However, as the size of the magnet increases, other contributions, such as the demagnetizing field created by the magnetization along with crystallographic defects and grains, start to factor in and the minimum energy configuration is no longer a uniform magnetization. The magnetic structure of a macroscopic ferromagnet thus consists of multiple *magnetic domains*, regions in which magnetization points uniformly in the same direction, separated by *domain walls*, regions where the magnetization changes smoothly from the direction of one domain to the direction of the other. The net magnetic moment of the ferromagnet is the sum of the magnetization in the individual domains. Applying an external field results in parallel aligned domains growing larger and other domains shrinking, resulting in strengthening the net magnetic moment in the direction of the applied field. When all the domains are aligned into a single direction, a material-dependent *saturation magnetization* is reached, and the magnetization of the magnet cannot be increased further.

1.2 Magnetic thin films

A particularly interesting class of magnets are ferromagnetic *thin films*, which are, in simple terms, films in which the thickness is considerably smaller than the other dimensions of the film. Hence what exactly constitutes as ”thin” might vary slightly from source to source, but in physical context this usually means the point at which the thin system starts exhibiting qualitatively different properties than a non-thin system. When it comes to magnetic thin films, absolute thicknesses below a few micrometers are usually considered to be thin [5, 6], with ultrathin films, having thick-

nesses of a few atomic layers [7, 8], typically being treated as a separate category.

Compared to bulk ferromagnets, thin films have very large surface area. This change in surface-to-volume ratio increases the relative importance of surface and interface effects, which can alter the magnetic properties, such as the saturation magnetization [9] and Curie temperature [10] of thin films compared to bulk matter. In addition to the reduced dimensionality, the thin film fabrication methods, such as magnetron sputtering [11] or molecular beam epitaxy [12], affect the crystalline structure, which has a significant influence on the electromagnetic properties of the film [13]. Modern fabrication techniques have made it possible to construct magnetic films composed of multiple different material layers, in which the coupling between the layers can result in further changes in magnetic properties [14] or novel effects such as the Dzyaloshinskii-Moriya interaction [15].

Ferromagnetic thin films are researched extensively due to their wide range of magnetic properties and dynamics [16, 17, 18], the most well-known being probably giant magnetoresistance (GMR), in which the electrical resistance of a magnetic multilayer changes depending on whether the magnetization in the different layers is parallel or antiparallel [19, 20]. Magnetic thin films have plenty of existing applications and great potential for novel nano- and microscale devices in multiple fields, such as data storage [16, 21], magnetostrictive and magnetoresistive sensing [22, 23], spintronics [24] and magnonics [25].

1.3 Non-contact friction

Changes in magnetization incur energy losses due to various coupling mechanisms between the spin degrees of freedom and the lattice [26]. The link between changing magnetization and energy dissipation is evidenced macroscopically by the existence of the hysteresis loop in magnetization processes, and has also been demonstrated experimentally at the atomic level with a spin-polarized scanning tunneling microscope moving magnetic and non-magnetic adatoms on a magnetic substrate [27]. In the experiment, significant change in force required to move the magnetic adatoms from an adsorption site to the next was observed, depending on the strength of the coupling of the spin of the atom and the tip and whether the adatom was magnetic or nonmagnetic (Fig. 1.1).

When the change in magnetization and the resulting energy losses are induced by the movement of the magnetic specimen, like in the aforementioned experiment, it is natural to call these losses *magnetic friction*. Magnetic friction is a form of *non-contact friction*, that is friction between two moving bodies not in direct contact, separated by a vacuum gap [28]. In general, non-contact friction is mediated by long-range electromagnetic

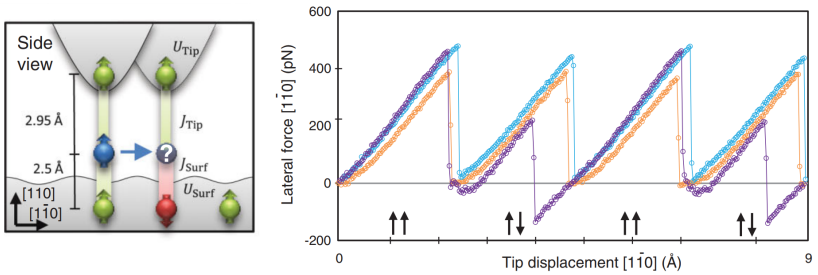

Figure 1.1. A schematic depiction of the experimental setup of moving adatoms on a magnetic substrate with a scanning tunneling microscope (left) and the lateral force exerted on the adatom coupled to tip of the microscope (right). The force depends on whether the adatom is non-magnetic (orange), weakly coupled to the tip (blue), or strongly coupled to the tip (purple). Reprinted from [27] with permission from American Physical Society.

interactions, including contributions from Van der Waals forces [29], Joule losses from electrostatic interactions [30] and local deformations of the surface leading to the creation of phonons [31].

Non-contact friction is usually very weak, the contribution in a typical sliding contact being about one billionth of the total friction force [32]. Thus non-contact friction forces are mainly considered in situations where one wants to minimize frictional energy loss. Magnetic losses in particular are a relevant contribution to overall energy loss in applications with alternating electromagnetic fields and/or components moving in such fields, such as in magnetic bearings [33], magnetic gears [34] and electric motors [35]. Additionally, a macroscale application utilizing non-contact friction forces can be found in eddy current brakes [36], though in this case the effect is usually referred to as eddy current damping rather than eddy current friction. Overall, if the strength of non-contact friction could be increased, it would be a desirable means of actuation and damping motion in systems that are normally susceptible to wear due to contact.

1.4 Thesis outline

The previous sections have introduced, in a general sense, the physical system and phenomena examined in this thesis. The remainder of the thesis is organized as follows: Chapter 2 describes ferromagnetic thin films and their magnetic dynamics, with focus on topological solitons studied in the publications. In Chapter 3, the theory behind magnetic losses is discussed from macroscopic and microscopic perspectives. Chapter 4 presents the theory of micromagnetism and practical considerations regarding micromagnetic simulations. Chapter 5 provides short summaries of the publications and an outlook.

2. Magnetic structure and dynamics of ferromagnetic thin films

Ferromagnetic thin films can be broadly separated into two classes: magnetically *hard* films, which are characterized by a preferred magnetization directions (*easy axes*) due to strong anisotropy induced by the crystalline structure (*magnetocrystalline anisotropy*), and magnetically *soft* films, where the magnetocrystalline anisotropy is largely absent and the magnetization aligns parallel to the film boundaries to minimize the *stray field* (or demagnetizing field), the magnetic field created by the magnetization of the ferromagnet itself [16]. The equilibrium magnetization and the magnetic dynamics of the two types of thin films differ considerably. Examples of ground state configurations of the two types of films, with dimensions 1 μm × 1 μm × 20 nm each, are shown in Fig. 2.1.

In hard magnetic thin films, the magnetic configuration is determined by the competition of three energy terms: the magnetocrystalline anisotropy energy, which is minimized when the magnetization points into the direction of the easy axis/axes, the stray field energy, which is minimized when magnetization direction aligns parallel to the boundaries of the magnet, and the exchange energy, which is minimized when all the magnetic moments are aligned in parallel to each other. Depending on the strength and direction of the magnetocrystalline anisotropy, the out-of-plane films can exhibit unique domain patterns such as bubble domains and maze-like domain structures [37]. Of especial interest are films in which the easy axis points out of the plane of the film, known as perpendicular (magnetic) anisotropy thin films, due to their potential applications in high-density data storage [38, 39].

In soft magnetic thin films, the magnetic structure is determined by the competition of the stray field energy and the exchange energy. For small films or nanodots (up to few tens of nanometers depending on the film/dot thickness [40]), the exchange interaction dominates and the ground state is a single magnetic domain [5]. In larger films, up to a couple of tens of microns [41], the stray field energy starts to compete with the exchange energy, causing the ground state configuration to depend on the geometry and topology of the film. Very high domain wall velocities have been

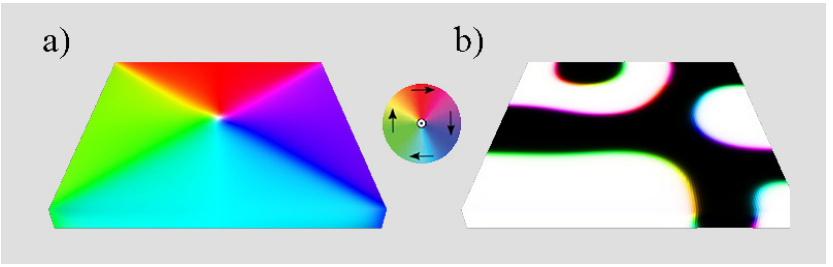

Figure 2.1. a) Magnetic equilibrium configuration of a monocrystalline Permalloy thin film with dimensions 1 µm × 1 µm × 20 nm, displaying the so-called *Landau pattern*, four domains separated by 90° domain walls and a single vortex at the center. **b)** A similarly sized CoCrPt thin film with out-of-plane uniaxial anisotropy, relaxed into a configuration with multiple up (white) and down (black) domains separated by domain walls. The color wheel at the center indicates the magnetization direction in the plane of the films.

reported in in-plane magnetized nanowires [42], making them promising candidates for domain wall memory and logic applications, the most famous concept probably being the magnetic domain wall racetrack memory [21].

2.1 Magnetic topological solitons

Due to the competition between the different energy terms, parts of the magnetization of a ferromagnet can form coherent magnetic configurations, which can be treated as non-linear solitary magnetization waves, i.e. *magnetic topological solitons* (also called magnetic topological defects) [43]. The term ”topological” here is attributed to the fact that theoretically, topological solitons cannot be transformed into a uniform field by any continuous deformation of the magnetization without surpassing an infinite energy barrier [44]. In real systems, the energy barrier is naturally never infinite, but nevertheless high enough to make the magnetic solitons remarkably stable. Topological solitons and their dynamics have garnered considerable scientific interest due to this stability, as they could potentially serve as nanoscale information carriers [45].

Topological solitons can be characterized by their *topological charge* Q (sometimes referred to as the skyrmion number)

$$Q = \frac{1}{4\pi} \iint \mathbf{m} \cdot \left(\frac{\partial \mathbf{m}}{\partial x} \times \frac{\partial \mathbf{m}}{\partial y} \right) d^2\mathbf{r},$$

where the integral is over the unit sphere, counting how many times the magnetization $\mathbf{m}$ wraps the unit sphere [46].

Depending on the thickness and magnetic properties of a ferromagnetic thin film, it can exhibit various types of solitons, including vortices, domain walls and skyrmions [47]. In this work, the main soliton/defect types

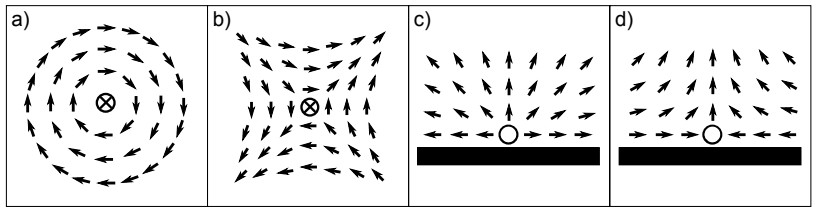

Figure 2.2. Schematic illustrations of the internal magnetic configurations of various point defects encountered in in-plane magnetic thin films: **a)** vortex **b)** antivortex and **c)** and **d)** edge defects. The circle indicates the core of the soliton, with out-of-plane polarization in the case of vortex and antivortex, and the black bar depicts the edge of the sample in **c)** and **d)**

encountered are vortices, antivortices, edge defects (or half-vortices) and domain walls, which will be discussed below. For research on skyrmions, see e.g. [48].

2.1.1 Vortices, antivortices and edge defects

Vortices, antivortices and edge defects are magnetic point defects/solitons that appear in thin films with weak magnetocrystalline anisotropy, such as Permalloy, where the magnetization prefers to align parallel to the boundaries of the magnet [49]. These point defects are characterized by small (approximately equal to the magnetic exchange length of the material) cores and fractional skyrmion numbers, $\pm 1/2$ for vortices and antivortices [50], and presumably $\pm 1/4$ for edge defects due to their half-vortex nature, though they're rarely discussed in the terms of topological charge. Schematic depictions of vortex, antivortex and two types of edge defect are provided in Fig. 2.2. Point defects and their dynamics in magnetically soft thin films are the focus of Publication I.

The core magnetization, often referred to as the polarization of the (anti)vortex, points out of the thin film plane [45]. In the case of vortices, the surrounding magnetization rotates around the core. Vortices are thus characterized by two quantities: the core polarization and the rotation direction of the surrounding magnetization (clockwise or counterclockwise). In antivortices, the magnetization around an antivortex does not rotate around the core of the defect, but instead points into the core from two opposite directions and out of the core from two perpendicular directions, with the rest of the surrounding magnetization assuming orientation in between these main directions.

The dynamics of vortices and antivortices, such as the gyrotropic motion of an isolated vortex in a nanodisk and the nucleation and annihilations of vortex-antivortex pairs, have been studied quite extensively [51, 52, 53, 54, 55]. It has been demonstrated that both the core polarization and the circulation of a vortex can be switched using high frequency field

pulses or spin-polarized currents [56, 57]. The polarization switching of a vortex core occurs through the forming of vortex-antivortex pair of opposing polarization and the annihilation of the original vortex and the antivortex, leaving only the vortex with different polarization [56]. This type of restricted pairwise nucleation and annihilation of vortices and antivortices is explained by the conservation of the skyrmion number [50]. Depending on the polarizations of the cores, the annihilation has been found to proceed either in a continuous, smooth manner or in a burst of spin-waves [58].

Vortices and antivortices are bulk defects, meaning they form in the bulk of the film and tend to stay away from the edges unless driven there due to e.g. magnetic relaxation or an outside influence such as an external magnetic field [49]. A third type of topological defect encountered in in-plane magnetized thin films, dubbed edge defects or half-vortices, are conversely confined to the edge and cannot move to the bulk. The edge defects are also different from vortices and antivortices in that the core magnetization of the defect does not necessarily point out of plane. Edge defects provide an additional skyrmion number conserving annihilation mechanism, in which a vortex annihilates with two edge defects [59].

In films with strong magnetocrystalline anisotropy, the formation of vortices and other point defects is suppressed due to the shape and topology of the magnet having less of an effect, as most of the magnetization is forced to point into the preferred direction(s). However, different kind of point defects can appear in these films, such as vertical Bloch lines that can form and move confined inside domain walls in films with perpendicular anisotropy, displaying similar nucleation and annihilation dynamics as vortices and antivortices [60], and edge dislocations, defects in stripe patterns of domain walls, with half-integer topological charges [61].

2.1.2 Domain walls

Domain walls are stable magnetic solitons in which magnetization rotates continuously between two domains. Two types of basic domain wall structure found in thin films, characterized by how the magnetization rotates along the wall relative to the wall direction, are Bloch walls, in which the magnetization rotates perpendicularly to the wall plane, and Néel walls, where the rotation is in the wall plane [5]. The two types of domain walls are illustrated in Fig. 2.3.

Bloch walls appear in bulk magnets and thin films with out-of-plane magnetocrystalline anisotropy. The width of the domain wall is determined by the competition between the exchange energy, attempting to align the magnetic moments, and the magnetocrystalline anisotropy energy, trying to align the magnetization along the preferred direction. Néel walls are typically found in very thin films and in films with weak magnetocrys-

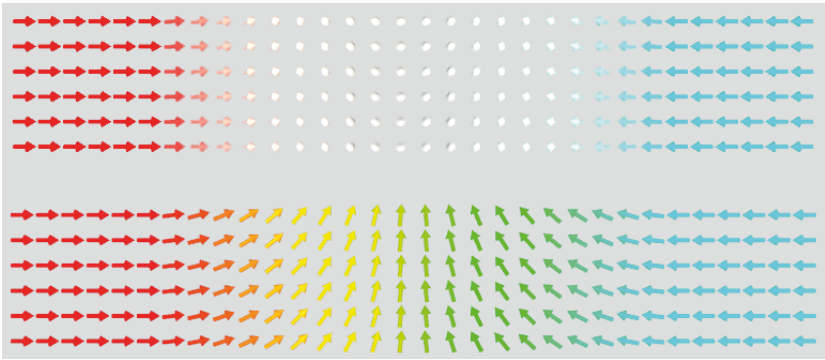

Figure 2.3. Illustrations of a 180° Bloch domain wall (upper), in which the magnetization rotates perpendicularly to the wall plane, and a 180° Néel domain wall (lower), in which the rotation occurs in the plane of the wall.

talline anisotropy, in which the wall width is restricted by the stray field energy. In addition to the classification in Bloch and Néel walls, domain walls are typically referred to by the degree of magnetization rotation from one domain to the other, with 180° and 90° domain walls being the most common.

Depending on the film geometry and the magnetocrystalline anisotropy strength and direction, the films can also exhibit domain walls with asymmetric and complex geometries, containing or being composed of topological defects. Sufficiently thick and wide in-plane magnetized strips, for example, exhibit vortex walls, where the wall is formed by one or more vortices [62]. Domain walls, mainly 180° Bloch domain walls in perpendicular anisotropy films, and their dynamics are the main focus of Publications III and IV.

2.2 Domain wall dynamics

When a multi-domain magnet is acted upon by an external field, magnetic domains in which the magnetization direction aligns with the external field expand while domains not aligned with the field shrink. The shrinking and expanding of domains is induces domain wall motion inside the magnet, leading to one of the simplest form of domain wall manipulation: driving via an applied field. Other novel methods of inducing domain wall motion have also been developed, including domain wall driving by spin-polarized currents, a process in which momentum is transferred from the current to the domain wall [63], and driving by electric fields, where the mechanism causing domain wall motion is based on elastic coupling between magnetic and ferroelectric domain walls in multiferroic heterostructures [64].

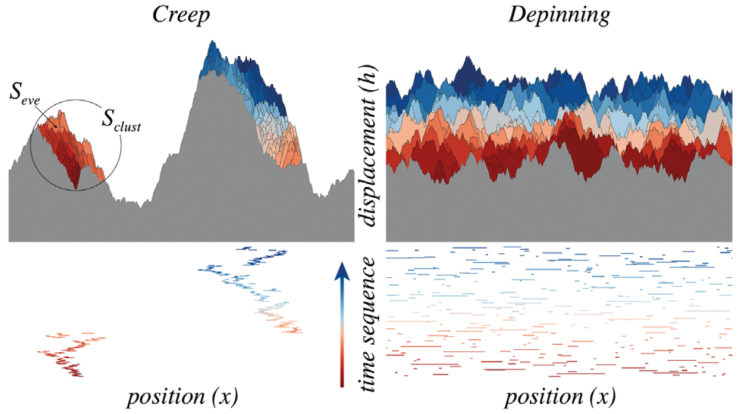

Figure 2.4. The time series of the displacement of a domain wall in the thermally activated creep regime (left) and at the depinning threshold (right). The time sequence is illustrated by a color code, from dark red (older) to dark blue (more recent). Reprinted from [66], with the permission of American Physical Society.

2.2.1 Domain wall motion in disordered media

Crystalline structures of solids found in nature are rarely perfect, but instead contain many kinds of impurities, crystallographic defects and grains. In this kind of disordered medium, domain walls can relax into energetically favorable locations, resisting the forces that attempt to move them, a phenomenon that is known as *domain wall pinning*. Domain wall pinning is responsible for many static properties of macroscopic magnets, such as coercivity and permeability [65].

A microscopic consequence of domain wall pinning is that the domain wall motion inside a ferromagnet is not continuous, but consists of periods of inactivity followed by short bursts of domain wall movement, during which the domain wall(s) rapidly jump from a low-energy configuration to another. The magnetic dynamics is thus dominated by intermittent domain wall jumps, the exact dynamics of which depend on the microstructure of the material and the strength of the driving relative to the critical *depinning field* H_{d}. Three kinds of domain wall motion have been distinguished: thermally activated *domain wall creep* below the depinning threshold, the *Barkhausen effect* exhibiting large avalanches of domain wall motion at driving close in magnitude to the depinning field, and *flow* or *sliding* regime when the depinning field is exceeded. The domain wall behavior during creep motion and at the depinning threshold are depicted in Fig. 2.4.

2.2.2 Creep motion

If the strength of the driving field is significantly below the depinning field, one finds the so-called domain wall creep regime. In this regime, the domain wall is mostly pinned, with small segments of the moving approximately independently, the motion being activated by random thermal fluctuations [67]. Creep motion has been experimentally observed in thin films and wires using magneto-optic Kerr effect [68] and extraordinary Hall effect [69], and investigated numerically with both micromagnetic simulations [70] and the Ising model [71].

In the creep regime, the average velocity of the domain wall follows an Arrhenius-like law $v \propto \exp(-U_\mathrm{p}/k_\mathrm{B}T \cdot (H/H_\mathrm{d})^\mu)$, where U_p is the characteristic pinning energy, T is the temperature, k_B is the Boltzmann constant [72]. The term $(H/H_\mathrm{d})^\mu$ represents scaling according to the driving field acting on the wall, with the value of the exponent μ depending on the by the dimension and the nature of the disorder in the system, initially understood through phenomenological arguments and later predicted by the renormalization group theory [73, 74]. Creep exponent values $\mu = 0.25$ and $\mu = 1$ typically found in experiments and simulations [67, 68, 69, 70, 71], corresponding to short-range and long-range disorder, respectively, generally agree well with the theoretical predictions.

The renormalization group theory predicts also that, like in the case of driving fields near the depinning threshold discussed in the next section, there's another class of domain wall creep in which the domain wall motion proceeds by collective avalanche-like dynamics [74]. These predictions have been confirmed by recent numerical simulations [66] and experimental work [75, 76].

2.2.3 The Barkhausen effect

When driven by fields close in magnitude to the depinning field, the motion of the domain wall occurs in wide avalanches, a phenomenon known as the *Barkhausen effect* [4]. The discontinuous domain wall motion results in a measurable (e.g. by winding a coil around a magnet and measuring the induced voltage during magnetization reversal) crackling noise signal called Barkhausen noise.

Barkhausen noise has been found to incorporate characteristics similar to many other kinds of crackling noise phenomena [77, 78]. For a wide range of avalanche sizes S, the size distribution follows a power law scaling with cutoff $P(S) \propto S^{-\tau_\mathrm{S}} f(S/S_0)$ where τ_S is the *critical exponent* for the avalanche size [79]. The cutoff is represented by a rapidly decaying function f with S_0 being the size cutoff value. The durations of the avalanches, T, have a similar distribution with its own critical exponent and cutoff.

Due to interest in the statistics of critical phenomena and avalanche dy-

namics in disordered systems, Barkhausen noise has been quite extensively studied, both in 3-dimensional [80] magnets and thin films [81, 82, 83, 84]. The power law distributions have been found to span a broad range of different materials, suggesting critical behavior in which the only the main symmetries and conservation laws influence the behavior of the system, while many other quantitative details are irrelevant. Two *universality classes* for have been identified, corresponding to the range of interactions governing the domain wall dynamics: long-range, in polycrystalline or partially crystallized amorphous alloys, governed by dipolar interactions, and short-range, in amorphous alloys, governed by short-range elastic interactions of the domain walls [85]. A temperature-induced crossover between the two universality classes has also been demonstrated [86].

Early experiments demonstrated various different values for τ_S and τ_T (see e.g. [87] and [88]), raising valid questions about the criticality and the universality classes in Barkhausen noise. As pointed out in [89], lengthy power law scaling sections can be obtained even without being directly at the critical point. Thus theoretical models of Barkhausen noise should include not only explanation for the power law scaling regions of e.g. the size distribution, but also an explanation for other statistical properties, such as the scaling relations of the cutoffs $S_0 \sim k^{-1/\sigma_k}$ and $T_0 \sim k^{-\Delta_k}$, where k is the demagnetizing factor representing a restoring force hindering the propagation of Barkhausen avalanches [90], and the scaling exponent relating the average avalanche size to the duration $\langle S(T)\rangle \sim T^{\gamma}$. The correctness of the predicted exponents can be verified using well-known scaling relations, e.g. $\gamma = (1-\tau_S)/(1-\tau_T)$ [80]. A model known as the ABBM model [91] was particularly successful for predicting the properties of systems with long-range disorder e.g. polycrystalline silicon steel, whereas short-range models are found suitable for amorphous systems [90].

2.2.4 Motion above the depinning field

When the driving field (or a current density threshold in the case of driving by spin-polarized current) is sufficient to overcome the pinning effects, $H > H_d$, the domain wall starts moving steadily on average, and its velocity becomes linearly dependent on the magnetic field or current density [92]. In addition to the strength of the driving, the velocity of the domain wall depends on the properties of the system, such as the type and width of the domain wall [93], the damping of magnetization of the material [94] and the dimensions of the film or strip [95].

The linear dependence continues until the strength of the driving field exceeds a certain material- and geometry-dependent threshold, the Walker field [96]. At this point the domain wall velocity starts to oscillate, causing the average domain wall velocity to experience a sudden drop. This phenomenon is called the Walker breakdown, a point at which the domain wall

motion becomes unstable due to the torque exerted by the driving influences overcoming the demagnetizing and damping fields [97]. In in-plane magnetic nanowires, the walker breakdown causes nucleation vortices and antivortices in the domain wall during motion, which slows down the propagation [55].

Above the Walker field, the domain wall starts to undergo precessional motion, leading to the wall velocity oscillations. When the driving field or current is further increased to high levels, the linear relationship between domain wall velocity and driving strength is regained, though the flow remains precessional and the mobility of the domain wall is greatly reduced [98]. As fast domain wall motion is highly desirable in spintronics applications, considerable effort has been made to understand how to enhance the velocity of domain walls and suppressing the Walker breakdown. Some of the proposed techniques include deliberately rough wire edges in magnetic strips [99] and having a perpendicular anisotropy layer underneath the in-plane layer [100], both of which suppress the nucleation of vortices and antivortices and show considerable enhancement in the domain wall velocity.

3. Magnetic losses

Heating up a magnetic sample causes excitations in the magnetization, eventually completely breaking down the magnetic order at the Curie temperature. This connection between lattice thermal excitations and the magnetic configuration goes both ways, and thus the relaxation of the magnetization also transfers energy from the spin excitations to the lattice. This chapter discusses the theoretical background of these magnetic losses from both macroscopic and microscopic perspectives.

3.1 Macroscopic losses

When a ferromagnet is magnetized cyclically into two opposite directions via an external field, the induced magnetic flux density **B** as a function of the external field strength **H** traces a loop (Fig. 3.1 **a**). The shape of the loop yields a great deal of information about the magnetic properties of the ferromagnet, such as magnetic saturation (the maximum extent to which the magnet can be magnetized), coercivity (the ability of the magnet to resist demagnetization) and remanence (the residual magnetization when the external field is removed) [2]. The area of the hysteresis loop expresses the amount of work lost as heat in one induction cycle. The losses can be divided into three separate contributions, P_{cl}, P_{h} and P_{exc}, which stand for classical loss, hysteresis loss and excess (or anomalous) loss, respectively (Fig. 3.1 **b**) [101]. In the case of a magnet in a sinusoidally oscillating field, the losses take the forms

$$P_{\mathrm{cl}} = \frac{\pi^2 \sigma d^2}{6}(Bf)^2, \quad P_{\mathrm{h}} = 4k_{\mathrm{hyst}} B^{\beta} f, \quad P_{\mathrm{exc}} = 1.63\frac{2L}{d}P_{\mathrm{cl}} \quad [\mathrm{Wm}^{-3}], \qquad (3.1)$$

where in the term P_{cl}, σ is the conductivity of the material, d is the thickness, B is the peak induction field and f is the frequency of the external field oscillation. Due to the strong dependence on the thickness and conductivity of the magnet, the classical losses are mostly neglibible in thin films and insulators [5]. The hysteresis loss per cycle of magnetization is independent of the magnetization frequency, leading in turn to a linear

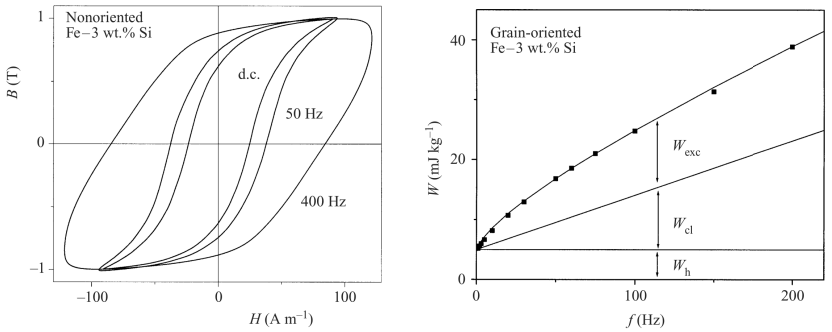

Figure 3.1. Hysteresis loops for a 0.35mm thick Fe–3wt.% Si lamination for a few different magnetization frequencies (left) and the three contributions to the magnetic losses for a grain-oriented 0.30mm thick Fe–3wt.% Si lamination (right). Reprinted from [101] with permission from Elsevier.

frequency dependence on the dissipation power as seen in the definition of P_{h}, where k_{hyst} and β are structural aspects affecting the domain wall pinning and magnetization reversal, their values depending on the material [101]. The equation for excess losses P_{exc}, where L is the average width of a domain, is valid for bar-like domains of varying widths [102].

Classical losses and excess (or anomalous) losses are essentially caused by Joule dissipation, in which eddy currents induced in a conducting magnet convert energy into heat. In this case, it is the currents and the resistivity of the conductor that are mostly responsible for the energy dissipation rather than the direct interaction of the magnetization and the lattice, and classical losses are present even without structural inhomogeneities and in single-domain particles without domain walls [101]. The excess losses, on the other hand, appear as the result of smooth large-scale motion of domain walls across the specimen, in which local eddy currents concentrate around the moving domain walls.

Hysteresis losses are a consequence of the pinning and depinning during domain wall motion discussed in Chapter 2, i.e. the fact that the motion of domain walls during the magnetization isn't smooth but proceeds in rapid jumps. The hysteresis losses are thus intimately tied to the degree of structural disorder in the material. In pure crystals, it's expected that hysteresis losses are negligible, whereas they are the main contributor to the energy dissipation in highly disordered materials. The losses studied in Publication IV are primarily hysteresis losses, whereas the excess losses are the main source of dissipation in Publication III due to the lack of structural disorder in the film(s).

3.2 Microscopic loss mechanisms

Though there is no general consensus on the complete nanoscale explanation for the magnetic relaxation and energy dissipation mechanisms as of yet, there are multiple pathways for the energy to be converted into heat through spin wave (magnon) interactions, such as magnon-phonon and magnon-electron interactions, magnon-impurity interactions, and magnon scattering on the surface and interface defects [26]. The dissipation channels can be broadly divided into two classes: intrinsic damping mechanisms, which are fundamental to a ferromagnetic material, and extrinsic damping mechanisms, which arise from inhomogeneous magnetization in multi-domain magnets and magnets with imperfections of the crystal structure, such as lattice defects and doping [103]. The total damping of the spin precession is the sum of these two contributions. The spin dynamics of various systems have been studied in ferromagnetic resonance (FMR) linewidth experiments [104, 105, 106], yielding insight to the intrinsic and extrinsic damping mechanisms.

3.2.1 Intrinsic damping

The intrinsic damping, also called Gilbert-type damping due to it being well described by the Landau-Lifshitz-Gilbert equation (see Chapter 4), is inherent to all kinds of ferromagnets, applying to bulk magnets and thin layers, and both electrically insulating and conducting magnets. A system exhibiting purely intrinsic damping would be a uniformly magnetized sample without lattice defects, the excitation being a uniform mode (wave vector k=0) magnon. The energy dissipation from this type of systems is thought to be mainly the result of spin-orbit coupling, which connects the precession of the magnetic moments to the lattice, and electron-hole pair creation and recombination, caused the by annihilation of uniform mode magnons [103]. The damping is thus dependent on the density of electronic states of the material, and the damping behavior as a function of temperature depends on whether the electron-hole pairs occupy the same energy band ("conductivity-like" damping, which increases with temperature) or different energy bands ("resistivity-like" damping, which decreases with temperature).

There are also various other mechanisms contributing to intrinsic damping which depend on the material. For example, in metallic magnets the exchange interaction of s-d electrons can be a major contributor to the damping [107], and impurities and doping can influence the intrinsic damping mechanisms through modifying the electron-magnon interaction. Another modification to the intrinsic damping can appear from an interface between ferromagnetic and nonmagnetic materials. At the interface, spin currents from the ferromagnetic layer can flow through into the nonmag-

netic layer, a phenomenon known as spin pumping [108], in which the spin angular momentum is transferred to the nonmagnetic layer and then dissipated, the transfer rate depending on the electronic configurations of the materials at the interface.

3.2.2 Extrinsic damping

The extrinsic damping effects include damping contributions that are not inherent properties of the material itself, but instead are the result of the structural inhomogeneities of the ferromagnet [104]. The inhomogeneities may arise from a multitude of microstructural origins, including magnetocrystalline anisotropy variation in a polycrystalline sample, magnetostriction coupled with nonuniform stresses, surface roughness, and step/edge anisotropy. Extrinsic damping is of theoretical and practical interest since it can be controlled by sample growth conditions and topology, making it possible to fabricate samples with a desired level of damping [109].

The mechanism behind extrinsic damping is usually attributed to the fact that the presence of the inhomogeneities in the magnetic structure make the magnetization precess in local resonant magnon modes instead of a uniform mode across the whole sample [103]. These non-uniform mode magnons can scatter from the uniform mode magnon or each other, a process referred to as two-magnon scattering [110], which is considered to be the main contributor of extrinsic damping. The scattering processes transfer energy from the uniform mode to non-uniform modes, which also interact with the other degrees of freedom of the lattice. This provides additional pathways for relaxation, leading to the enhancement of the damping, experimentally observable through the broadening of FMR resonance peak [111].

Like the uniform mode magnon, the non-uniform magnon modes can interact with the impurities and defects of the lattice. Thus, similar to the intrinsic damping, the extrinsic damping can be enhanced with doping [112] and in multilayer systems through the interlayer interaction [113].

3.3 Magnetic non-contact friction

When a magnetic surface moves in an external field or relative to another magnet, the magnetization interacts with the external field or the magnetic field of the magnet, respectively. The interaction transfers kinetic energy to magnetic excitations, which then transfer the energy to the lattice in the way described in the previous sections. This type of magnetic non-contact friction has been studied computationally in models with e.g. single spin moving atop a monolayer of spins, used to study temperature and velocity

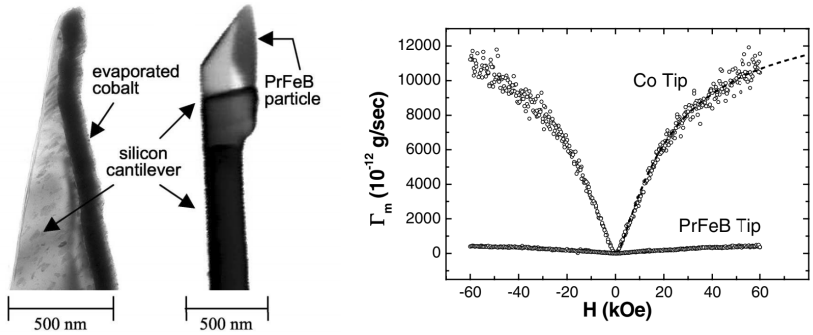

Figure 3.2. (**Left**) Transmission electron micrograph of a cobalt nanowire tip and a scanning electron micrograph of a Pr2Fe14B particle tip used to measure magnetic dissipation in an external field. (**Right**) The measured cantilever damping vs applied field for both tips. Reprinted from [120] with permission from American Physical society.

dependence of magnetic friction when the dynamics of the spins follow the Landau-Lifshitz-Gilbert equation [114, 115]. Both velocity independent (Coulomb) friction and velocity dependent (Stokes) magnetic friction have been demonstrated in these simulations, though the difference in frictional behavior could be explained by the simulation model [116].

Studies regarding two larger-scale interacting magnetic surfaces have been more rare, likely due to the large computational cost involved. One such study, using Monte Carlo simulations in the Ising model [117], displaced a half-plane of a two-dimensional Ising square lattice parallel across the other half-plane. In this model, it was found that the magnetic friction force is highest near the Curie temperature, and that antiferromagnetic coupling lead to stronger friction than ferromagnetic coupling. However, the study was more akin to contact friction due to exchange interaction being the main contributor to friction. Using scalar approximation for the magnetic moments and thin domain wall approximation [118], an investigation of a larger-scale model with two disordered thin films incorporating stripe domains and interacting with dipolar interactions has been performed [119]. In this study, various regimes of domain wall and film motion, such as stick slip and domain wall dragging, were found.

There have also been some experimental studies regarding magnetic friction, though experiments are relatively rare due to the challenges in detecting the small friction forces. In addition to the single atom spin-flipping experiment discussed in the introduction, magnetic friction has been demonstrated experimentally using a soft cantilever with a magnetic tip oscillating in an external magnetic field [120]. In strong (approaching 6 T) external magnetic fields, the damping coefficient measured for a cobalt tip were found to be in the $10^{-13} - 10^{-12}$ kg/s range (Fig. 3.2). The importance of magnetic degrees of freedom to the energy loss was illustrated by

showing that the dissipation was material dependent, with magnetically more malleable cobalt showing orders of magnitude higher dissipation compared to the stronger anisotropy PrFeB, for which the damping didn't differ significantly from the damping of a bare silicon (i.e. non-magnetic) cantilever.

4. Micromagnetics

The central theory and framework used in all the publications I-IV is micromagnetics, specifically micromagnetic dynamics simulations. This chapter aims to provide the necessary details on both the theoretical and computational aspects of micromagnetics essential to this work.

4.1 Basics of micromagnetic theory

Micromagnetism is a semiclassical continuum theory of magnetism, in which the atomic details are ignored and the magnetization is treated as a continuous vector field inside a magnetic sample, the interactions of the magnetic moment vectors with external influences and each other being described by various *effective field* terms. The micromagnetic theory gained tract after it was established and generally accepted that the magnetization of ferromagnets consisted of magnetic domains separated by domain walls, as *ab initio* methods were (and to a large extent still are) unfeasible in analyzing the domain structure and dynamics of microscale magnets. Continuum expressions for the exchange energy [121] and the anisotropy energy [122] were derived in the 1930s and 1940s along with the equations of motion for the magnetic moments, and the basic principles and methods of micromagnetics were collected into a single whole by Brown in 1963 [123]. Nowadays, micromagnetics has become the standard tool for research involving magnetostatics and -dynamics at length scales between atomistic spin dynamics (< 1 nm) and domain theory (1 μm - 1 mm) [5]. Falling into the realm of micromagnetics are thus particles which are large enough to be nonuniformly magnetized (but small enough to not contain regular domain patterns studied in domain theory), and the inner structure and dynamics of magnetic substructures such as domain walls and skyrmions. Hence, micromagnetic theory is particularly apt for analyzing magnetic structure and dynamics in magnetic thin films and strips.

4.1.1 Micromagnetic energy

The central problem that micromagnetics aims to solve is finding the magnetization **M** of a sample of arbitrary shape in thermodynamic equilibrium. This is done by finding the minimum of the total magnetic Gibbs free energy G, which can be expressed as volume integral of the sum of the energy densities of different magnetic interactions [124]

$$G = \int_V \left[A(\nabla \mathbf{m})^2 + \varepsilon_{\text{anis}} - \mu_0 M_\text{s}(\mathbf{H}_\text{ext} \cdot \mathbf{m}) - \frac{1}{2}\mu_0 M_\text{s}(\mathbf{H}_\text{demag} \cdot \mathbf{m}) + \varepsilon_\text{me} \right] \, dr^3, \quad (4.1)$$

where V is the volume of the magnet and **m** is the magnetization normalized by the saturation magnetization, $\mathbf{m} = \mathbf{M}/M_\text{s}$. The above expression contains the five energy density terms most commonly present in magnetic materials (in the order they appear in the equation): the exchange energy, magnetocrystalline anisotropy energy, Zeeman (external field) energy, demagnetizing field energy and magnetoelastic energy. Some of the energy terms were already discussed in Chapter 2, but they're also are briefly explained here. For a more thorough description, see e.g. [124].

Exchange energy density $A(\nabla \mathbf{m})^2$ is the result of the quantum mechanical exchange interaction driving neighboring spins into aligning with each other. The exchange stiffness constant A, indicating the strength of the exchange interaction, is usually determined experimentally, and for common ferromagnetic materials is in the range $1-10$ pJ/m [5]. As can be seen from the energy expression, the exchange energy is minimized when the magnetization is aligned uniformly in one direction.

The magnetocrystalline anisotropy energy density $\varepsilon_{\text{anis}}$ originates from the spin-orbit coupling and depends on the crystal structure of the material. The existence of magnetocrystalline anisotropy results in preferred directions of the magnetization, called easy axes or directions. In the simplest case of uniaxial anisotropy materials, such as the ones simulated in the publications III and IV of this work, the magnet has a single easy axis with a single anisotropy constant K_u. In this case, the magnetocrystalline anisotropy energy density assumes the form $\varepsilon_{\text{anis}} = K_\text{u}(\mathbf{m} \cdot \mathbf{u})$, where **u** is the uniaxial anisotropy direction vector.

The external (or applied) field and the demagnetizing field energies $\mu_0(\mathbf{H}_\text{ext} \cdot \mathbf{M})$ and $\frac{1}{2}\mu_0(\mathbf{H}_\text{demag} \cdot \mathbf{M})$ arise directly from the interaction of the magnetization with the external and demagnetizing fields, respectively, being at a minimum when the magnetization points along the field lines. The demagnetizing field or stray field is the magnetic field produced by the magnetization itself, directly derivable from the Maxwell's equations. The stray field is generated by magnetic volume and surface "charges", analogous to electric field arising from electric charges [125]. Thus, in order to minimize stray field energy, the individual magnetic moments close to the surface of the magnet tend to align parallel to the surface.

Magnetoelastic energy $\varepsilon_{\mathrm{me}}$ comes from the interaction between elastic stresses and the magnetization of the magnet. Due to the relatively low (Publication I) and fabrication method dependent (Publications II-IV) magnetoelastic energies of the thin films studied in this work, the contribution of magnetoelasticity is neglected.

4.1.2 Brown's equations and the effective field

Below the Curie temperature and in thermal equilibrium, the saturation magnetization M_{s} stays constant. Thus only the direction of the magnetization, represented by the normalized magnetization $\mathbf{m} = \mathbf{M}/M_{\mathrm{s}}$, varies. The equilibrium magnetization state is then found at a point where the first-order variation of G with respect to $\mathbf{m}$ is zero, leading to the equation [126]

$$\begin{aligned}\delta G = &\int_V \left(-2\nabla\cdot(A\nabla\mathbf{m}) + \frac{\delta\varepsilon_{\mathrm{anis}}}{\delta\mathbf{m}} - \mu_0 M_{\mathrm{s}}\mathbf{H}_{\mathrm{d}} - \mu_0 M_{\mathrm{s}}\mathbf{H}_{\mathrm{ext}}\right)\delta\mathbf{m}\ dV \\ &+ \int_{\partial\Omega} \left(2A\frac{\partial\mathbf{m}}{\partial n}\cdot\delta\mathbf{m}\right)\ dS = 0,\end{aligned} \tag{4.2}$$

where $\partial\mathbf{m}/\partial n$ is the normal derivative of the magnetization. The variation $\delta\mathbf{m}$ is of the form $\delta\bar{\theta}\times\mathbf{m}$, which represents an arbitrarily small rotation $|\delta\bar{\theta}|$ about the direction of the vector $\delta\bar{\theta}$ [123]. Using the vector calculus identity $\mathbf{v}\cdot(\delta\bar{\theta}\times\mathbf{m}) = \delta\bar{\theta}\cdot(\mathbf{v}\times\mathbf{m}) = -\delta\bar{\theta}\cdot(\mathbf{m}\times\mathbf{v})$, one obtains

$$\begin{aligned}\delta G = &\int_V \mathbf{m}\times\left(2\nabla\cdot(A\nabla\mathbf{m}) - \frac{\delta\varepsilon_{\mathrm{anis}}}{\delta\mathbf{m}} + \mu_0 M_{\mathrm{s}}\mathbf{H}_{\mathrm{d}} + \mu_0 M_{\mathrm{s}}\mathbf{H}_{\mathrm{ext}}\right)\cdot\delta\bar{\theta}\ dV \\ &+ \int_{\partial\Omega}\left(2A\frac{\partial\mathbf{m}}{\partial n}\times\mathbf{m}\right)\cdot\delta\bar{\theta}\ dS = 0.\end{aligned} \tag{4.3}$$

Since $\delta\bar{\theta}$ is an arbitrary rotation, the variation can be zero if and only if

$$\begin{cases}\mathbf{m}\times\left(2\nabla\cdot(A\nabla\mathbf{m}) - \frac{\delta\varepsilon_{\mathrm{anis}}}{\delta\mathbf{m}} + \mu_0 M_{\mathrm{s}}\mathbf{H}_{\mathrm{d}} + \mu_0 M_{\mathrm{s}}\mathbf{H}_{\mathrm{ext}}\right) = 0 \\ 2A\frac{\partial\mathbf{m}}{\partial n}\times\mathbf{m}\big|_{\partial\Omega} = 0\end{cases},$$

the conditions can be written in a simpler form by introducing the effective field $\mathbf{H}_{\mathrm{eff}}$, which encompasses the various field terms,

$$\mathbf{H}_{\mathrm{eff}} = \frac{1}{\mu_0 M_{\mathrm{s}}}2\nabla\cdot(A\nabla\mathbf{m}) - \frac{1}{\mu_0 M_{\mathrm{s}}}\frac{\delta\varepsilon_{\mathrm{anis}}}{\delta\mathbf{m}} + \mathbf{H}_{\mathrm{d}} + \mathbf{H}_{\mathrm{ext}},$$

and noting that the normal derivative $\partial\mathbf{m}/\partial n$ is orthogonal to $\mathbf{m}$ in the second condition, thus meaning that the normal derivative has to be zero. Together, these yield elegant equilibrium conditions for the magnetization,

$$\begin{cases}\mu_0 M_{\mathrm{s}}\mathbf{m}\times\mathbf{H}_{\mathrm{eff}} = 0 \\ \frac{\partial\mathbf{m}}{\partial n}\big|_{\partial\Omega} = 0\end{cases},$$

known as Brown's equations. They state that in equilibrium, magnetization is parallel to the direction of the effective field, and that the normal derivative of the magnetization at the surface vanishes. The second condition can be modified in the presence of surface and interlayer anisotropies [5].

4.2 Dynamic micromagnetics

In addition to finding the magnetization configuration in equilibrium, micromagnetic theory is also capable of handling magnetization dynamics, which consists of the magnetic moments precessing around and relaxing into the direction of the effective field. Dynamic micromagnetics has been utilized to interpret and investigate e.g. magnetic switching [127] and ferromagnetic resonance [128], among other rapid magnetic processes.

4.2.1 The Landau-Lifshitz-Gilbert equation

The key to solving micromagnetic dynamics is finding the appropriate equation of motion for the magnetic moments. The first considerations by Bloch [129] analyzed the time-dependent motion of uncoupled and undamped magnetic moments, treating the motion as classical mechanical precession. Landau and Lifshitz published an equation of motion for magnetic moments with damping in 1935 [121], the Landau-Lifshitz equation

$$\frac{d\mathbf{M}}{dt} = -\gamma_0(\mathbf{M}\times\mathbf{H}_{\text{eff}}) - \frac{\lambda}{M_{\text{s}}^2}\left(\mathbf{M}\times(\mathbf{M}\times\mathbf{H}_{\text{eff}})\right), \tag{4.4}$$

in which the first term of the equation describes the precessional motion of the magnetization $\mathbf{M}$ around the effective field $\mathbf{H}_{\text{eff}}$, with a frequency determined by the gyromagnetic constant $\gamma_0 = |\gamma|\mu_0 \approx 221$ kHz/(Am^{-1}), where γ is the electron gyromagnetic ratio and μ_0 is the permeability of vacuum. The second term describes the winding down of the precession, λ being the dimensionless Landau-Lifshitz damping constant. The precessional motion of the magnetic moment around H_{eff} with the precession and damping terms is depicted in Fig. 4.1.

In 1955, Gilbert pointed out that the Landau-Lifshitz equation is valid only for small damping and proposed an alternative damping term [130], leading to the Landau-Lifshitz-Gilbert (LLG) equation

$$\frac{d\mathbf{M}}{dt} = -\gamma_0(\mathbf{M}\times\mathbf{H}_{\text{eff}}) + \frac{\alpha}{M_{\text{s}}}(\mathbf{M}\times\frac{d\mathbf{M}}{dt}), \tag{4.5}$$

where α is the Gilbert damping constant, representing the damping influences acting on the magnetic moments discussed in Chapter 3. The Gilbert damping constant is usually determined from ferromagnetic resonance or time-resolved magneto-optical Kerr effect experiments [131]. The LLG

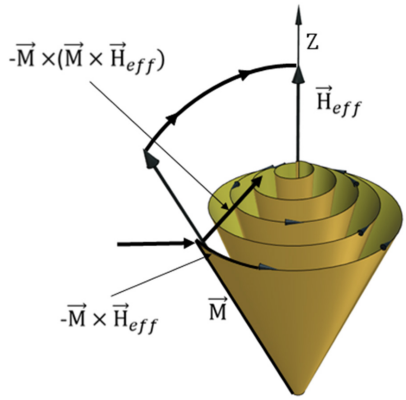

Figure 4.1. A schematic image of the precession dynamics of a spin according to the LLG equation, with the terms responsible for the precession and damping indicated by vectors. Reprinted from [103] with permission from IOP Publishing.

equation can be cast into the mathematically equivalent Landau-Lifshitz form

$$\frac{d\mathbf{M}}{dt} = -\gamma_0^*(\mathbf{M}\times\mathbf{H}_{\text{eff}}) - \frac{\lambda^*}{M_{\text{s}}^2}\big(\mathbf{M}\times(\mathbf{M}\times\mathbf{H}_{\text{eff}})\big), \tag{4.6}$$

where the gyromagnetic terms γ_0^* and γ_0 and damping constants λ^* and α are related by

$$\gamma_0^* = \frac{\gamma_0}{1+\alpha^2}, \qquad \lambda^* = \frac{\alpha\gamma_0 M_{\text{s}}}{1+\alpha^2},$$

respectively. Due to the equivalence, both Eqs. (4.4) and (4.5) are commonly referred in literature as the Landau-Lifshitz-Gilbert equation, and both equations produce the same dynamics when the damping is weak.

The LLG equation has become the staple of dynamic micromagnetics, with further extensions to the basic equation having been developed to deal with additional effective field terms representing various excitations and interactions, e.g. thermal fluctuations [132], spin-polarized currents [133] and the Dzyaloshinskii-Moriya interaction [134].

4.3 Micromagnetic simulations

The micromagnetic equations in general are difficult to treat analytically in all but the simplest of systems. As such, numerical micromagnetics is often the tool of choice when it comes to research concerning magnetic domains and their dynamics. Since their early application in predicting domain wall structure in soft thin films [135], micromagnetic simulations have been used to reproduce a variety of experimental results in a multitude of systems, see e.g. [136, 137, 138]. With the advances in GPU-accelerated

computing, the speed of micromagnetic simulations has surged [139, 140], making it possible to perform larger length- and timescale simulations, µm and µs by the time of writing of this thesis.

Finite element methods (FEM) and finite difference methods (FDM) have been found well-suited for solving micromagnetic problems [141]. Both methods are based on discretizing the magnetic volume of interest into small subvolumes and solving the LLG equation in each subvolume, which are cuboid (often cubic) cells in FDM and tetrahedra in FEM. As such, finite element methods are usually suitable for problems involving curved geometries, while finite difference methods tend to be advantageous in rectangular geometries and in problems with large surface area. Since the publications in this thesis concern rectangular thin films, FDM was the natural choice. The simulations of this work are performed with the open-source micromagnetic code Mumax3 [142].

In an FDM micromagnetic simulation, the individual discretization cells of the magnet are typically treated as uniformly magnetized, represented by a vector in each cell. These magnetization vectors interact with the local effective field $\mathbf{H}_{\text{eff}}$ in the discretization cells, also assumed uniform per cell, and revolve in time according to the LLG equation. The time discretization is typically handled by adaptive step algorithms, in which the step size is adjusted according to the local truncation error. Thus the timestep can be reduced during rapid events (such as vortex-antivortex annihilations) and increased when the change in magnetization is slower, saving computation time compared to fixed step algorithms while retaining good accuracy. The spatial discretization is limited by the exchange length l_{ex} [5], below which the magnetization direction can be considered uniform. The exchange length is determined by $l_{\text{ex}} = \sqrt{A/K}$, i.e. the exchange constant A and the appropriate magnetocrystalline anisotropy constant K. Having a discretization cell size close to or above the exchange length can introduce numerical problems, such as artificial pinning of domain walls, to the simulation. In thin films with weak magnetocrystalline anisotropy, another exchange length, the magnetostatic exchange length $l_{\text{mex}} = \sqrt{2A/(\mu_0 M_{\text{s}}^2)}$, can become a limiting factor [143]. In this case, the Néel domain walls typical to this type of systems cannot be resolved properly unless the discretization cell is smaller than the magnetostatic exchange length.

4.3.1 GPU acceleration and the demagnetizing field

Most of the effective field terms in the micromagnetic equations are local and efficient to solve numerically. However, the demagnetizing field term represents a non-local long range interaction, through which all the magnetic moments interact with each other, making the micromagnetic simulations scale as N^2 with the number of magnetic moments. This results in the demagnetizing field calculation usually being the most com-

putationally heavy part of micromagnetic simulations, a fact due to which a considerable effort has been made to make the calculation of the demagnetizing fields more efficient. A discussion of the techniques is presented e.g. in [144].

One of these techniques, usable in FDM micromagnetics and used by Mumax3, is utilizing Fast Fourier Transforms (FFT) to speed up the evaluation of the demagnetizing field. The technique is based on the fact that on a regular simulation grid, the demagnetizing field components of an individual magnetic moment can be reduced into geometric coefficients, hence making it possible to write the demagnetizing field calculation as a convolution of the magnetization and a demagnetizing (field) kernel, a 3-by-3 tensor [125]. The convolution can then be transformed from real space to a pointwise multiplication of the Fourier transformed magnetization and the demagnetizing kernel, reducing the calculation complexity from $O(n^2)$ to $O(n \log n)$ of Fast Fourier transforms. Both the FFT and the pointwise multiplication can be calculated using Graphics Processing Units (GPU), massively parallelizing the operations for increased simulation speed. The demagnetization tensor can be calculated once at the beginning of the simulation, Fourier transformed and moved to the GPU, while the magnetization has to be transformed and inverse-transformed during each time step, the number of transforms being dependent on the time integration scheme used. The Fourier transformation and GPU acceleration are important in Publication II, as these methods restrict the calculation of the demagnetizing field to specific points, requiring interpolation in order to find the demagnetizing field at any point in space.

4.4 Energy loss in micromagnetic simulations

Micromagnetic simulations have been employed to study the magnetic losses in single domain particles and nanowires, with the dissipation in magnetic switching of nanomagnets receiving particular attention due to possible applications in magnetic logic devices [145, 146, 147]. In micromagnetism, the Gilbert damping constant incorporates the microscopic energy loss mechanisms discussed in Chapter 3, with the micromagnetic calculations inherently including the energy transfer to various spin-wave modes, and the damping term consisting only of energy loss mechanisms that transfer energy out of the system [148]. The rigorous evaluation of the value of the Gilbert damping constant is difficult due to the variety of the damping mechanisms and the challenge in separating the intrinsic and extrinsic damping effects. There is also discussion over whether the simple constant form of the damping is appropriate for modeling the energy dissipation [149].

The phenomenology of the damping term considered by Gilbert, in which

the damping torques can be derived from a Rayleigh dissipation function [150], leads to a relation between the time derivative of the magnetization and the energy dissipation

$$\frac{dW}{dt} = \eta \int_V \left(\frac{d\mathbf{M}}{dt}\right)^2 = \frac{\alpha\mu_0}{\gamma_0 M_\mathrm{s}} \int_V \left(\frac{d\mathbf{M}}{dt}\right)^2 dr^3.$$

Inserting the LLG equation from (4.5) in place of the derivative $\partial\mathbf{M}/\partial t$, one has

$$\frac{dW}{dt} = \frac{\alpha\mu_0}{\gamma_0 M_\mathrm{s}} \int_V \left[\frac{\gamma_0}{1+\alpha^2}\left(\mathbf{H}_\mathrm{eff} \times \mathbf{M} + \frac{\alpha}{M_\mathrm{s}}\mathbf{M} \times (\mathbf{M} \times \mathbf{H}_\mathrm{eff})\right)\right]^2 dr^3,$$

which, due to the orthogonality of the precession and damping terms, becomes

$$\frac{dW}{dt} = \frac{\alpha\mu_0\gamma_0}{(1+\alpha^2)^2 M_\mathrm{s}} \int_V (\mathbf{H}_\mathrm{eff} \times \mathbf{M})^2 + \frac{\alpha^2}{M_\mathrm{s}^2}\left(\mathbf{M} \times (\mathbf{M} \times \mathbf{H}_\mathrm{eff})\right)^2 dr^3.$$

Finally, noting that $\left(\mathbf{M} \times (\mathbf{M} \times \mathbf{H}_\mathrm{eff})\right)^2$ is equal to $M_\mathrm{s}^2(\mathbf{H}_\mathrm{eff} \times \mathbf{M})^2$ yields a simple form

$$\begin{aligned}\frac{dW}{dt} &= \frac{\alpha\mu_0\gamma_0}{(1+\alpha^2)^2 M_\mathrm{s}} \int_V (1+\alpha^2)(\mathbf{H}_\mathrm{eff} \times \mathbf{M})^2 \, dr^3 \\ &= \frac{\alpha\mu_0\gamma_0}{(1+\alpha^2) M_\mathrm{s}} \int_V (\mathbf{H}_\mathrm{eff} \times \mathbf{M})^2 \, dr^3\end{aligned}$$

In finite difference micromagnetics, the magnet is typically discretized into cells of equal volume, with $\mathbf{M}$ and $\mathbf{H}_\mathrm{eff}$ being constant in each cell. In such a system, the total dissipation power is just a sum over the dissipation in individual cells:

$$\frac{dW}{dt} = \frac{\alpha\mu_0\gamma_0 V_\mathrm{cell}}{(1+\alpha^2) M_\mathrm{sat}} \sum_{i=1}^{N} \left(\mathbf{M}_\mathrm{i} \times \mathbf{H}_\mathrm{eff,i}\right)^2, \tag{4.7}$$

where V_cell is the volume of the discretization cell. This form for the dissipation power is used in the calculations of Publications III and IV.

5. Summaries of the publications

5.1 Publication I

Publication I focuses on the coarsening dynamics of topological solitons and the resulting energy dissipation in permalloy thin films after a rapid quench from an initially random magnetization. Similar phase-ordering kinetics, in which the density of topological defects has often been found to follow power law decay, has been studied in various kinds of systems, including liquid crystals, biosystems and cosmology. In magnetic context, such coarsening dynamics have been previously studied in Ising and XY-models, but less so in the framework of micromagnetism with realistic material parameters and all the relevant magnetic interactions included.

We use micromagnetic simulations to investigate the relaxation dynamics of 20 nm thick permalloy films with lateral sizes ranging from 512 nm to 4096 nm. At the beginning of each simulation, the film is set to a randomized magnetization, mimicking a high-temperature paramagnetic configuration, and is let relax in time without external influences and in zero temperature. After a short initial fluctuation phase, stable topological point defects discussed in Chapter 2, vortices, antivortices, and edge defects, form and exhibit coarsening dynamics through mutual annihilation of colliding defects. We implement a method to identify and track the motion of the different types of defects from the magnetization data, following the defect dynamics as well as quantities such as the total winding number of the system and the counts of the defects.

Monitoring the defect dynamics during the relaxation, we detect various winding number conserving annihilation and core switching events. We find that the density of each kind of defect follows a power law with an exponent depending on the defect type, with the exponent values deviating from those found previously for simpler magnetic models. As the defects are main contributors to the total energy of the film, the total energy of the system also follows a power law decay during the defect annihilation phase

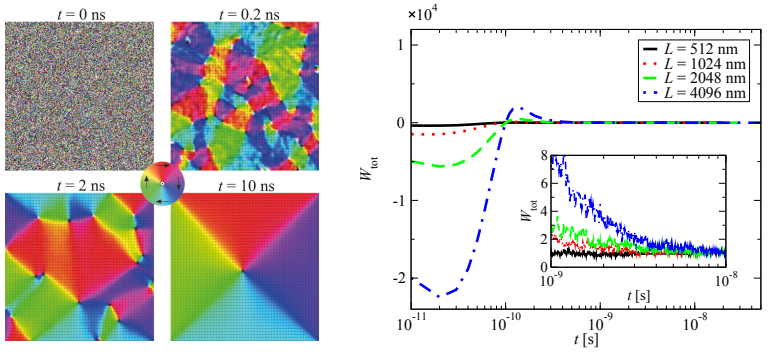

Figure 5.1. (Left) Four snapshots of a 1024 nm × 1024 nm × 20 nm Permalloy film undergoing relaxation from an initially random magnetization state at $t = 0$ to single-vortex state at $t = 10$ ns. **(Right)** The converging of the winding number towards 1 for the different film sizes, with large initial deviations due to the magnetic fluctuations making defects difficult to detect.

of the relaxation. The final relaxation of the system typically occurred as single vortex gyration, eventually stopping at the center of the film, though some simulated films ended up in metastable states with two or more topological defects.

We also investigate the effect of the Gilbert damping parameter α and quenched disorder on the relaxation, and find that high α tends to lead to lower values for the power law exponents for all defect types, approaching the value obtained from the XY-model with linear damping and short range interactions only. The quenched disorder was realized by dividing the films into grains via Voronoi tessellation with 20 nm average grain size, and varying the saturation magnetization in each grain or decreasing the strength of exchange between grains. We found that the disorder had a negligible effect on the decay exponents.

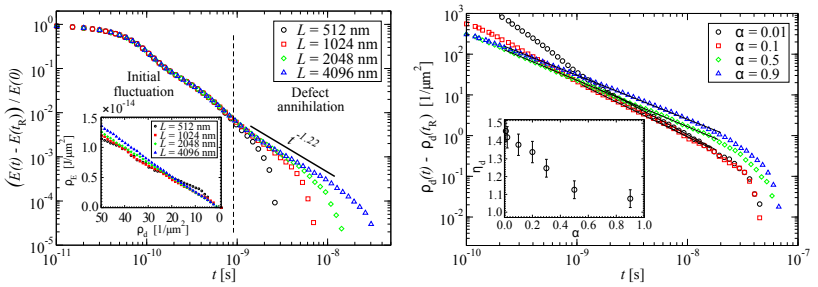

Figure 5.2. (Left) The time evolution of the energy during relaxation in Permalloy films of various sizes, showing the initial fluctuation stage of relaxation and the stage dominated by defect annihilation. The inset shows the energy as a function of point defect density. **(Right)** The total defect densities for different values of the Gilbert damping constant α. The inset shows the decrease of the decay exponent as a function of α.

5.2 Publication II

In Publication II we develop an extension to an existing micromagnetic framework, Mumax3, with the aim of studying magnetic domain dynamics in thin films stimulated by motion, either in an external field or relative to another film. The main focus of the extension is simulating two interacting thin films, one of which is driven in a specified direction with either constant velocity or attached to a spring moving at a constant velocity, while the other film remains in place. Using the extension, one can simulate e.g. the tip-sample interaction in magnetic force microscopy and non-contact friction between sliding magnetic surfaces, the latter being the subject of interest of Publications III and IV.

In a simulation scenario with two thin films separated by more than a few nanometers, the films interact through their demagnetizing fields. As discussed in Chapter 4, the demagnetizing field calculation is normally an $O(n^2)$ operation in the number of simulation cells, due to which in Mumax3 the calculation is sped up using Fast Fourier transforms (FFTs). With the FFT method, the demagnetizing field calculation can be accomplished as a pointwise multiplication between the Fourier transformed magnetization and a kernel consisting of geometric coefficients, the latter of which can be computed once at the beginning of simulation and stored on the GPU. This reduces the computational complexity to $O(n \log n)$, significantly speeding up the computation.

However, due to a fixed demagnetization kernel, using the FFT method means that the demagnetizing field can only be calculated in a single predefined point (usually in the center) of each discretization cell. With moving films, this leads to discrete motion and jumps in the demagnetizing field experienced by both films, which further causes discontinuities in e.g. the total energy of the system.

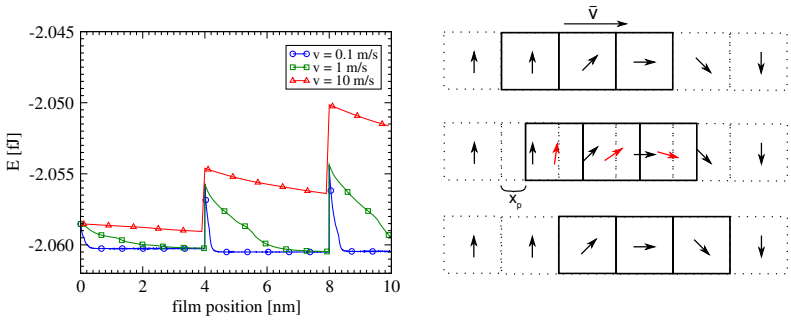

Figure 5.3. **(Right)** The artificial discontinuations in the energy due to a film moving one discretization cell at a time for three different velocities. The motion causes an immediate magnetic excitation, which then relaxes, best seen at the lowest velocity. **(Left)** Schematic idea of the interpolation of a magnetic field vectors inside a discretized magnet moving between the discretization cells.

We solve the discontinuity problem by implementing two methods of smoothly interpolating the demagnetizing field terms in between the finite difference discretization cells: direct interpolation of the field vectors, and the calculation of the demagnetizing field through magnetic scalar potential. Both methods utilize cubic B-spline interpolation on the GPU, due to cubic B-splines being twice continuously differentiable, a physical requirement for the magnetic scalar potential. In addition to the demagnetizing field, the applied external field vectors can also be interpolated directly in the case of simulations where an external field is applied.

We assess our implementation with an example simulation of stick-slip motion, where two stripe-patterned CoCrPt films are sliding relative to each other, one of the films being pulled by a spring. We observe continuous domain and stray field evolution, smoothed by the spline interpolation, leading to continuous energy, spring force and other quantities. Due to the interpolation, however, some undesirable artificial divergence and curl of the demagnetizing field are inevitably introduced to the system. Fortunately, testing both the direct interpolation and the scalar potential methods for a field created by a random magnetization, we find that the artificial divergence and curl are increased relatively little (less than one thousandth) compared to the baseline numerical noise already present in the system.

In addition to the movement code, we implemented a method to explicitly calculate the eddy current field induced by the changing magnetization. The method was tested by simulating the magnetic switching of a Permalloy nanocube, where we studied how the eddy current field and the Gilbert damping parameter influence the switching time. The effect of eddy currents was found to be somewhat dependent on the Gilbert damping, and overall quite modest in this scenario.

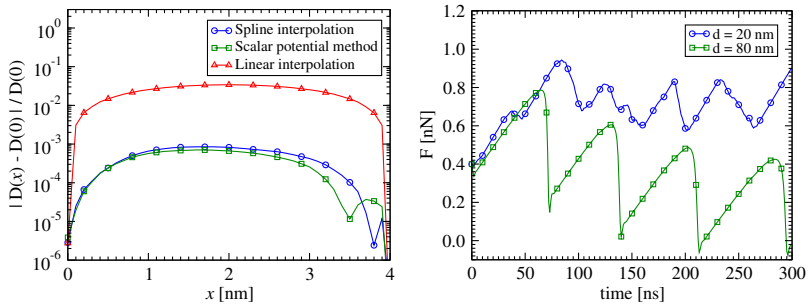

Figure 5.4. (Left) The percentage increase in artificial divergence due to the interpolated magnetic field for different methods of calculation, showing how the spline interpolation and the scalar potential method lead to significantly smaller increase in artificial divergence compared to linear interpolation. **(Right)** The spring force in the numerical example simulation for two values of distance d between the films, showing stick slip motion with the higher distance.

5.3 Publication III

In Publication III we use the extension developed in Publication II to study magnetic non-contact friction. Compared to other forms of non-contact friction touched upon in the Introduction, the magnetic interactions and their contribution to the energy dissipation having seen comparatively little research. Hence Publication III focuses on the magnetic friction due to domain dynamics in magnetic thin films. In particular, we're interested in the energy dissipation arising from domain wall motion.

Experimentally, non-contact friction is usually studied with ring-down measurements, in which the oscillations of an oscillator, typically a cantilever, are damped due to non-contact friction forces. In this type of measurement, the slowly winding down oscillations of the cantilever can be modeled as damped harmonic oscillation, where the exponential decay of the amplitude occurs both due to the internal damping of the cantilever and the non-contact frictional damping. From the amplitude decay, one can find the the damping coefficient Γ, and separating the internal damping gives the strength of the damping due to non-contact friction, usually found to be in the $\Gamma \approx 10^{-12} - 10^{-14}$ kg/s range.

In Publication III, we perform micromagnetic simulations of ring-down measurements, the studied systems being perpendicular anisotropy thin films oscillating in space due to being coupled with a spring. We employ two simulation setups, one with a single thin film oscillating in an external field, and another mimicking a magnetic cantilever tip oscillating atop a magnetic substrate with 20 nm distance in between, such that the interaction of the tip and the substrate occurs through their stray fields. Both films have a simple domain configuration of two out-of-plane domains pointing in opposite directions, with a single Bloch domain wall in between. We alter various micromagnetic material parameters of the films, such as the saturation magnetization, the strength of the uniaxial magnetocrystalline anisotropy and the Gilbert damping parameter, observ-

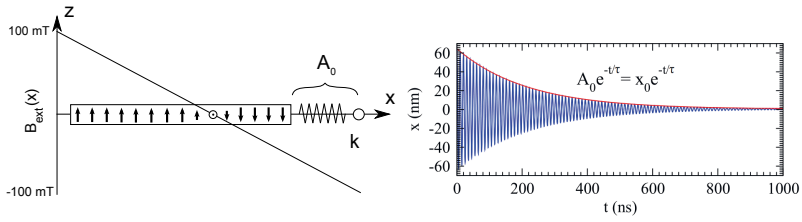

Figure 5.5. (Left) A schematic visualization of a simulation setup consisting of a single thin film oscillating in an external field, with two domains aligned along the easy axis, and a Bloch domain wall in between the domains **(Right)** The winding down of the amplitude in a ring down simulation of a single film, with oscillation frequency f_0 = 112 MHz.

ing how these parameters influence the domain wall dynamics and the energy dissipation.

From the results of our simulations, we distinguish three separate dynamic regimes for the domain wall motion, accompanied with different domain wall behavior and correspondingly different damping coefficients. Depending on the parameters, the domain wall(s) can move smoothly and rigidly or with fluctuations and internal excitations such as Bloch lines nucleating within. It's also possible for the studied systems to become completely in-plane polarized, e.g. in the case of strong exchange interaction and weak magnetocrystalline anisotropy. In the regime characterized by domain wall excitations and fluctuations, the domain wall motion and the damping coefficient is especially susceptible to the frequency of the oscillation, with the frequency dependence being pronounced in the tip-substrate system.

The material parameter simulations were performed with frequencies of 56 MHz or 112 MHz, which are relatively high compared to experimental cantilever frequencies. Hence, we further investigated the frequency dependence of the damping coefficient, performing simulations in the motion regime where the domain wall motion is smooth. Going from 56 MHz down to 8 Mhz, we observe that the damping coefficient is unaffected by frequency when below roughly 40 MHz. In this regime, the domain wall moves as an approximately rigid object, in which case the micromagnetic losses as formulated by Brown, discussed in Chapter 4, also predict a frequency-independent damping coefficient. Overall, we find the damping of the simulated systems at the simulated frequencies to be of roughly the same order of magnitude as other forms of non-contact friction found in literature.

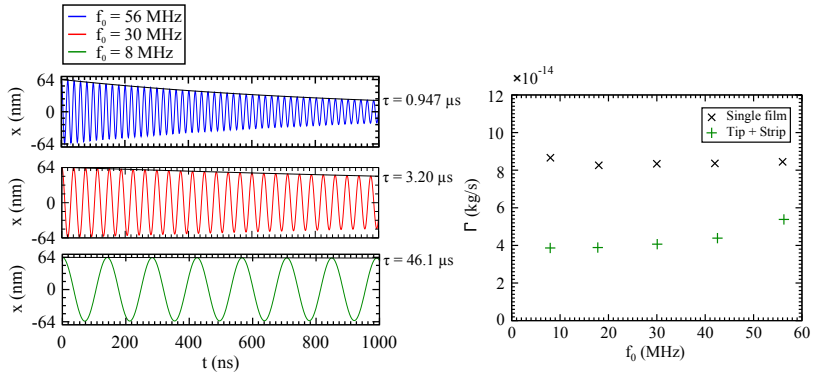

Figure 5.6. (Left) The decay of the amplitude with time in the single thin film setup for three different oscillation frequencies, with the decay constants τ marked on the right for each frequency. **(Right)** The damping coefficients Γ for the two simulation setups for various frequencies, showing weak to nonexistent frequency dependence below ≈ 40 MHz.

5.4 Publication IV

Publication IV considers the effects of polycrystalline structure and disorder on domain wall dynamics and magnetic friction. We study the domain wall pinning and the resulting intermittent avalanche-like bursts of domain wall motion discussed in Chapter 2 via numerical simulations, again using Mumax3 with the extension of Publication II. In this case the simulated system consists of two 20 nm thick polycrystalline CoCrPt films with out-of-plane magnetocrystalline anisotropy, set up in a magnetic configuration of two domains with domain walls in between. Like in the second setup of Publication III, the films are set 20 nm apart and interact only with their demagnetizing fields. The upper film is driven forward with a constant velocity, with periodic boundary conditions in the driving direction.

The polycrystallinity of the films is realized through Voronoi tessellation and perturbing the direction of the magnetocrystalline anisotropy vector from the out-of-plane direction by small amount in each grain. We examine the influence of the disorder by varying both the average grain diameter and the extent of the magnetocrystalline anisotropy vector deviations, representing the strength of the disorder. As the domain wall width in the studied films is approximately 22 nm, we consider grains with average diameter that is smaller (10 nm), roughly as large (20 nm), and larger (40 nm) than the domain wall width. We also test the effects of driving velocity ($v = 0.1 - 10$ m/s) and the width of the films ($w = 20 - 1200$ nm).

When measuring the average energy dissipation during motion, we find that the energy losses are significantly increased compared to monocrystalline systems studied in Publication III. Compared to the smooth domain

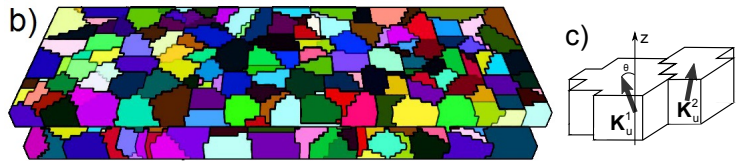

Figure 5.7. **a)** The two films and the initial magnetization configuration (periodic images not shown). The color wheel shows the orientation of the in-plane magnetization. **b)** The schematic depiction of the Voronoi tessellated grains of the two films. **c)** The realization of the disorder: anisotropy vectors with randomized deviations from the $z-$axis in a pair of grains.

wall motion with weak to nonexistent disorder, the energy dissipation (i.e. magnetic friction) in a strongly disordered system was approximately an order of magnitude higher. The strength of magnetic friction is at its peak when the domain wall motion is dominated by frequent large avalanches, a regime which is reached with different strength of disorder for each grain size. If the strength of the disorder is too high, however, the domain walls can become completely pinned, leading vanishing energy dissipation due to the magnetization not changing in response to the motion.

Increasing the width of the film increases the magnitude of the magnetic friction in a nonlinear fashion at small sizes, likely due to system-wide domain wall avalanches and strong dependence on the grain configuration when there are only few grains along the domain wall. The increase becomes linear after the film can accommodate 14 – 20 grains. The velocity dependence is linear throughout the tested values (0.2 m/s – 10 m/s), corresponding to hysteresis losses discussed in Chapter 3. At higher velocities, the domain walls could experience a breakdown, leading to single domain films and vanishing friction.

The domain wall roughness and the size distribution of domain wall avalanches, which resembled a power over one decade after which there was a rapid cutoff, were found to match quite well to domain wall creep motion statistics found in literature, even though the driving is caused by the interaction between the films instead of thermal activation responsible for the avalanches in the creep regime. The duration distribution was found to resemble a log-normal distribution, with an average avalanche duration of 11 ns. The stray field interaction limited the extent of the domain wall avalanches, likely explaining the cutoff of the size distribution and the short average avalanche duration. The film width and the driving velocity did not significantly affect the avalanche distributions.

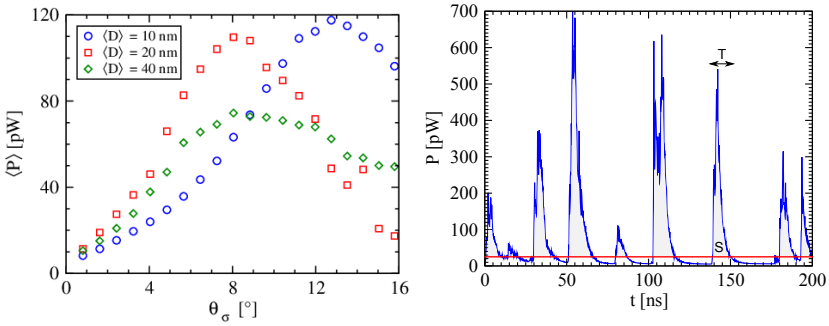

Figure 5.8. (Left) The average dissipation power during motion as a function of the strength of the disorder for each grain size. The results for high disorder has more noise, due to strong pinning resulting in fewer but larger avalanches. **(Right)** The power dissipation signal as a function of time for a $w = 400$ nm system driven with $v = 1$ m/s, showing multiple avalanches with varying sizes (S) and durations (T). The red line is the avalanche threshold.

5.5 Outlook

Non-contact friction is still a relatively young subfield of nanotribology, with plenty of systems to study and phenomena to uncover. The main contributions of this thesis are providing a method to investigate magnetic non-contact friction with simulations in the full micromagnetic picture, and laying the groundwork with studies on magnetic friction in out-of-plane systems with domain walls. Magnetic friction originating from the interaction of topological defects in in-plane magnetized thin films like those studied in Publication I was also planned, but unfortunately had to be cut due to time constraints.

Though large-scale applications of magnetic non-contact friction are unlikely due to the difficulty of controlling the structure and the magnetization of macroscopic magnets, magnetic friction could have potential in microscale applications e.g. in MEMS and NEMS. An advantage of magnetic friction compared to e.g. electrostatic and phononic friction is the robustness regarding surface contamination, and the fact that the strength of magnetic interactions between surfaces could be adjusted using external magnetic fields. In addition to utilizing magnetic interactions for manipulating mechanical motion, understanding magnetic friction is important in the cases where one wants to minimize external damping influences in a system, such as in force and displacement sensors.

As is usual with purely computational work, experimentally investigating systems similar to those studied in this thesis would be crucial to verify or debunk the results of the simulations. In fact, one of the major obstacles encountered while working on the dissertation was the scarcity of existing research with which to compare results. Naturally, performing experiments involving such weak forces is challenging. Particularly interesting would be experimental work on large thin films with multiple interacting domains and domain walls, as the strength of magnetic friction would likely be increased to more easily measurable levels. In general, identifying the magnitudes of the different damping contributions that are incorporated in the Gilbert damping constant in micromagnetic simulations, such as eddy currents and intrinsic and extrinsic damping, would clarify the role of the magnetic contribution to non-contact friction.

Further computational work is also not difficult to come up with. In addition to simulating in-plane thin films and the magnetic friction due to interaction of topological defects, the extension developed for Mumax3 could be used to study adhesion and stick-slip dynamics. The avalanche statistics found in Publication IV and their dependence on e.g. grain size and the driving method could also be investigated more thoroughly.

References

[1] A. Goldman. Applications and functions of ferromagnetic materials. In *Handbook of Modern Ferromagnetic Materials*, pages 1–15. Springer US, Boston, MA, 1999.

[2] G. Bertotti. *Hysteresis in Magnetism: For Physicists, Materials Scientists, and Engineers*. Electromagnetism. Elsevier Science, 1998.

[3] The magnetic field. In *The Physical Principles of Magnetism*, chapter 1, pages 1–30. John Wiley & Sons, Ltd, 2013.

[4] B. D. Cullity and C. D. Graham. *Introduction to Magnetic Materials*. Wiley-IEEE Press, 2 edition, 2008.

[5] A. Hubert and R. Schäfer. *Magnetic Domains: The Analysis of Magnetic Microstructures*. Springer Berlin Heidelberg, 2008.

[6] J.P. Volkerts. *Magnetic Thin Films: Properties, Performance, and Applications*. Condensed matter research and technology series. Nova Science Publishers, Incorporated, 2011.

[7] J.A.C. Bland and B. Heinrich. *Ultrathin Magnetic Structures I: An Introduction to the Electronic, Magnetic and Structural Properties*. Ultrathin Magnetic Structures. Springer Berlin Heidelberg, 2006.

[8] B. Heinrich and J. F. Cochran. Magnetic ultrathin films. In *Handbook of Magnetism and Advanced Magnetic Materials*. Wiley, 2007.

[9] F. Eskandari, S. B. Porter, M. Venkatesan, P. Kameli, K. Rode, and J. M. D. Coey. Magnetization and anisotropy of cobalt ferrite thin films. *Phys. Rev. Materials*, 1:074413, Dec 2017.

[10] P.J. Jensen, H. Dreyssé, and K.H. Bennemann. Thickness dependence of the magnetization and the Curie temperature of ferromagnetic thin films. *Surface Science*, 269-270:627 – 631, 1992.

[11] M. Ozimek, W. Wilczyński, and B. Szubzda. Magnetic thin film deposition with pulsed magnetron sputtering: deposition rate and film thickness distribution. *IOP Conference Series: Materials Science and Engineering*, 113:012009, Feb 2016.

[12] J. Cheng, V. K. Lazarov, G. E. Sterbinsky, and B. W. Wessels. Synthesis, structural and magnetic properties of epitaxial MgFe2O4 thin films by molecular beam epitaxy. *Journal of Vacuum Science & Technology B: Microelectronics and Nanometer Structures Processing, Measurement, and Phenomena*, 27(1):148–151, 2009.

[13] U. Gradmann. Magnetism in ultrathin transition metal films. volume 7 of *Handbook of Magnetic Materials*, pages 1–96. Elsevier, Dec 1993.

[14] J. Camarero, T. Graf, J. J. de Miguel, R. Miranda, W. Kuch, M. Zharnikov, A. Dittschar, C. M. Schneider, and J. Kirschner. Surfactant-mediated modification of the magnetic properties of Co/Cu(111) thin films and superlattices. *Phys. Rev. Lett.*, 76:4428–4431, Jun 1996.

[15] D. Khadka, S. Karayev, and S. X. Huang. Dzyaloshinskii-Moriya interaction in Pt/Co/Ir and Pt/Co/Ru multilayer films. *Journal of Applied Physics*, 123(12):123905, 2018.

[16] T. Thomson. Magnetic properties of metallic thin films. In *Metallic Films for Electronic, Optical and Magnetic Applications: Structure, Processing and Properties*, pages 454–546. Dec 2014.

[17] F. J. Himpsel, J. E. Ortega, G. J. Mankey, and R. F. Willis. Magnetic nanostructures. *Advances in Physics*, 47(4):511–597, 1998.

[18] Y. M. Kim, S. H. Han, H. J. Kim, D. Choi, K. H. Kim, and J. Kim. Thickness effects on magnetic properties and ferromagnetic resonance in Co-Ni-Fe-N soft magnetic thin films. *Journal of Applied Physics*, 91(10):8462–8464, 2002.

[19] M. N. Baibich, J. M. Broto, A. Fert, F. Nguyen Van Dau, F. Petroff, P. Etienne, G. Creuzet, A. Friederich, and J. Chazelas. Giant magnetoresistance of (001)Fe/(001)Cr magnetic superlattices. *Phys. Rev. Lett.*, 61:2472–2475, Nov 1988.

[20] G. Binasch, P. Grünberg, F. Saurenbach, and W. Zinn. Enhanced magnetoresistance in layered magnetic structures with antiferromagnetic interlayer exchange. *Phys. Rev. B*, 39:4828–4830, Mar 1989.

[21] S. Parkin, M. Hayashi, and L. Thomas. Magnetic domain-wall racetrack memory. *Science*, 320(5873):190–194, 2008.

[22] T. Calkins, A. Flatau, and M. Dapino. Overview of magnetostrictive sensor technology. *Journal of Intelligent Material Systems and Structures*, 18:1057–1066, Oct 2007.

[23] D.J. Mapps. Magnetoresistive sensors. *Sensors and Actuators A: Physical*, 59(1):9 – 19, 1997. 1st European magnetic sensors and actuators conference.

[24] G.C. Lombardi and G.E. Bianchi. *Spintronics: Materials, applications and devices*. Jan 2009.

[25] V. V. Kruglyak, S. O. Demokritov, and D. Grundler. Magnonics. *Journal of Physics D: Applied Physics*, 43(26):260301, Jun 2010.

[26] M. Fähnle and D. Steiauf. Dissipative magnetization dynamics close to the adiabatic regime. In *Handbook of Magnetism and Advanced Magnetic Materials*. Wiley, 2007.

[27] B. Wolter, Y. Yoshida, A. Kubetzka, S. Hla, Ki. von Bergmann, and R. Wiesendanger. Spin friction observed on the atomic scale. *Phys. Rev. Lett.*, 109:116102, Sep 2012.

[28] E. Gnecco and E. Meyer. *Elements of Friction Theory and Nanotribology*. Cambridge University Press, 2015.

[29] A. I. Volokitin and B. N. J. Persson. Theory of the interaction forces and the radiative heat transfer between moving bodies. *Phys. Rev. B*, 78:155437, Oct 2008.

[30] W. Denk and D. W. Pohl. Local electrical dissipation imaged by scanning force microscopy. *Applied Physics Letters*, 59(17):2171–2173, 1991.

[31] B. Gotsmann. Sliding on vacuum. *Nature Materials*, 10:87 EP –, Jan 2011.

[32] M. Kisiel, M. Samadashvili, U. Gysin, and E. Meyer. Non-contact friction. In Seizo Morita, Franz J. Giessibl, Ernst Meyer, and Roland Wiesendanger, editors, *Noncontact Atomic Force Microscopy: Volume 3*, pages 93–110. Springer International Publishing, Cham, 2015.

[33] D. C. Meeker, A. V. Filatov, and E. H. Maslen. Effect of magnetic hysteresis on rotational losses in heteropolar magnetic bearings. *IEEE Transactions on Magnetics*, 40(5):3302–3307, Sep. 2004.

[34] M. Desvaux, H. Bildstein, B. Multon, H. Ben Ahmed, S. Sire, A. Fasquelle, and D. Laloy. Magnetic losses and thermal analysis in a magnetic gear for wind turbine. In *2018 Thirteenth International Conference on Ecological Vehicles and Renewable Energies (EVER)*, pages 1–7, April 2018.

[35] J. Lee, Y. Kim, S. Rhyu, I. Jung, S. Chai, and J. Hong. Hysteresis torque analysis of permanent magnet motors using preisach model. *IEEE Transactions on Magnetics*, 48(2):935–938, Feb 2012.

[36] D. Ma and J. Shiau. The design of eddy-current magnet brakes. *Transactions of the Canadian Society for Mechanical Engineering*, 35, Mar 2011.

[37] H. Knüpfer, C. B. Muratov, and F. Nolte. Magnetic domains in thin ferromagnetic films with strong perpendicular anisotropy. *Archive for Rational Mechanics and Analysis*, 232(2):727–761, May 2019.

[38] G. Mathew, E. Hwang, J. Park, G. Garfunkel, and D. Hu. Capacity advantage of array-reader-based magnetic recording (ARMR) for next generation hard disk drives. *IEEE Transactions on Magnetics*, 50(3):155–161, March 2014.

[39] S. N. Piramanayagam. Perpendicular recording media for hard disk drives. *Journal of Applied Physics*, 102(1):011301, 2007.

[40] K. L Metlov and K. Y. Guslienko. Stability of magnetic vortex in soft magnetic nano-sized circular cylinder. *J. Magn. Magn. Mater.*, 242:1015–1017, 2002.

[41] K. Y. Guslienko. Magnetic vortex state stability, reversal and dynamics in restricted geometries. *J. Nanosci. Nanotechnol.*, 6:2745–2760, 2008.

[42] D. Atkinson, D. A. Allwood, G. Xiong, M. Cooke, C. Faulkner, and R. Cowburn. Magnetic domain-wall dynamics in a submicrometre ferromagnetic structure. *Nature materials*, 2:85–7, Mar 2003.

[43] V. G. Baryakhtar, M. V. Chetkin, S. N. Gadetskii, and B. A. Ivanov. *Dynamics of topological magnetic solitons experiment and theory*. Springer tracts in modern physics. Springer, Berlin, 1994.

[44] H. Braun. Topological effects in nanomagnetism: from superparamagnetism to chiral quantum solitons. *Advances in Physics*, 61(1):1–116, 2012.

[45] R. Tomasello, A. Giordano, V. Puliafito, and M. Carpentieri. Magnetic solitons driven by spin-based phenomena: A review on their features and potentialities. In *2015 IEEE 1st International Forum on Research and Technologies for Society and Industry Leveraging a better tomorrow (RTSI)*, pages 177–180, Sep. 2015.

[46] N. Nagaosa and Y. Tokura. Topological properties and dynamics of magnetic skyrmions. *Nature nanotechnology*, 8:899–911, Dec 2013.

[47] J. Seidel, R. K. Vasudevan, and N. Valanoor. Topological structures in multiferroics - domain walls, skyrmions and vortices. *Advanced Electronic Materials*, 2(1):1500292, 2016.

[48] A. Fert, N. Reyren, and V. Cros. Magnetic skyrmions: Advances in physics and potential applications. *Nature Reviews Materials*, 2, Jun 2017.

[49] O. Tchernyshyov and G. Chern. Fractional vortices and composite domain walls in flat nanomagnets. *Phys. Rev. Lett.*, 95(19):197204, 2005.

[50] O. A. Tretiakov and O. Tchernyshyov. Vortices in thin ferromagnetic films and the skyrmion number. *Phys. Rev. B*, 75:012408, Jan 2007.

[51] K. Lee and S. Kim. Gyrotropic linear and nonlinear motions of a magnetic vortex in soft magnetic nanodots. *Applied Physics Letters*, 91(13):132511, 2007.

[52] J. Shibata and Y. Otani. Magnetic vortex dynamics in a two-dimensional square lattice of ferromagnetic nanodisks. *Phys. Rev. B*, 70:012404, Jul 2004.

[53] K. Lee and S. Kim. Two circular-rotational eigenmodes and their giant resonance asymmetry in vortex gyrotropic motions in soft magnetic nanodots. *Phys. Rev. B*, 78:014405, Jul 2008.

[54] T. Shinjo, T. Okuno, R. Hassdorf, K. Shigeto, and T. Ono. Magnetic vortex core observation in circular dots of permalloy. *Science*, 289(5481):930–932, 2000.

[55] M. Hayashi, L. Thomas, C. Rettner, R. Moriya, and S. Parkin. Direct observation of the coherent precession of magnetic domain walls propagating along permalloy nanowires. *Nature Physics*, 3:21–25, Dec 2006.

[56] S. Kim, Y. Choi, K. Lee, K. Y. Guslienko, and D. Jeong. Electric-current-driven vortex-core reversal in soft magnetic nanodots. *Applied Physics Letters*, 91(8):082506, 2007.

[57] V. Uhlír, M. Urbánek, L. Hladík, J. Spousta, M. Im, P. Fischer, N. Eibagi, J. Kan, E. Fullerton, and T. Sikola. Dynamic switching of the spin circulation in tapered magnetic nanodisks. *Nature nanotechnology*, 8, Apr 2013.

[58] R. Hertel and C. M. Schneider. Exchange explosions: Magnetization dynamics during vortex-antivortex annihilation. *Phys. Rev. Lett.*, 97(17):177202, 2006.

[59] S. D. Sloetjes, E. Digernes, F. K. Olsen, R. V. Chopdekar, S. T. Retterer, E. Folven, and J. K. Grepstad. Interplay between bulk and edge-bound topological defects in a square micromagnet. *Applied Physics Letters*, 112(4):042401, 2018.

[60] T. Herranen and L. Laurson. Domain walls within domain walls in wide ferromagnetic strips. *Phys. Rev. B*, 92:100405, Sep 2015.

[61] S. Fin, R. Silvani, S. Tacchi, M. Marangolo, L.-C. Garnier, M. Eddrief, C. Hepburn, F. Fortuna, A. Rettori, M. G. Pini, and D Bisero. Straight motion of half-integer topological defects in thin Fe-N magnetic films with stripe domains. *Scientific Reports*, 8, Dec 2.018.

[62] V. Estévez and L. Laurson. Head-to-head domain wall structures in wide permalloy strips. *Phys. Rev. B*, 91:054407, Feb 2015.

[63] A. Thiaville, Y. Nakatani, J. Miltat, and N. Vernier. Domain wall motion by spin-polarized current: a micromagnetic study. *Journal of Applied Physics*, 95(11):7049–7051, 2004.

[64] K. J. A. Franke, B. Van de Wiele, Y. Shirahata, S. J. Hämäläinen, T. Taniyama, and S. van Dijken. Reversible electric-field-driven magnetic domain-wall motion. *Phys. Rev. X*, 5:011010, Feb 2015.

[65] G. Herzer. Grain size dependence of coercivity and permeability in nanocrystalline ferromagnets. *IEEE Transactions on Magnetics*, 26(5):1397–1402, Sep. 1990.

[66] E. E. Ferrero, L. Foini, T. Giamarchi, A. B. Kolton, and A. Rosso. Spatiotemporal patterns in ultraslow domain wall creep dynamics. *Phys. Rev. Lett.*, 118:147208, Apr 2017.

[67] S. Lemerle, J. Ferré, C. Chappert, V. Mathet, T. Giamarchi, and P. Le Doussal. Domain wall creep in an Ising ultrathin magnetic film. *Phys. Rev. Lett.*, 80:849–852, Jan 1998.

[68] P. J. Metaxas, J. P. Jamet, A. Mougin, M. Cormier, J. Ferré, V. Baltz, B. Rodmacq, B. Dieny, and R. L. Stamps. Creep and flow regimes of magnetic domain-wall motion in ultrathin Pt/Co/Pt films with perpendicular anisotropy. *Phys. Rev. Lett.*, 99:217208, Nov 2007.

[69] F. Cayssol, D. Ravelosona, C. Chappert, J. Ferré, and J. P. Jamet. Domain wall creep in magnetic wires. *Phys. Rev. Lett.*, 92:107202, Mar 2004.

[70] L. D. Geng and Y. M. Jin. Domain wall creep in magnetic thin films near the depinning transition. *EPL (Europhysics Letters)*, 116(3):36002, Nov 2016.

[71] R. H. Dong, B. Zheng, and N. J. Zhou. Creep motion of a domain wall in the two-dimensional random-field Ising model with a driving field. *EPL (Europhysics Letters)*, 98(3):36002, May 2012.

[72] W. Kleemann. Universal domain wall dynamics in disordered ferroic materials. *Annual Review of Materials Research*, 37(1):415–448, 2007.

[73] P. Chauve, T. Giamarchi, and P. Le Doussal. Creep via dynamical functional renormalization group. *Europhysics Letters (EPL)*, 44(1):110–115, Oct 1998.

[74] P. Chauve, T. Giamarchi, and P. Le Doussal. Creep and depinning in disordered media. *Phys. Rev. B*, 62:6241–6267, Sep 2000.

[75] V. Repain, M. Bauer, J.-P. Jamet, J. Ferré, A. Mougin, C. Chappert, and H. Bernas. Creep motion of a magnetic wall: Avalanche size divergence. *Europhysics Letters (EPL)*, 68(3):460–466, Nov 2004.

[76] M. P. Grassi, A. B. Kolton, V. Jeudy, A. Mougin, S. Bustingorry, and J. Curiale. Intermittent collective dynamics of domain walls in the creep regime. *Phys. Rev. B*, 98:224201, Dec 2018.

[77] J. P. Sethna, K. A Dahmen, and C. R. Myers. Crackling noise. *Nature*, 410(6825):242–250, 3 2001.

[78] A. Vespignani, H. Stanley, and S. Zapperi. Plasticity and avalanche behaviour in microfracturing phenomena. *Nature*, 388:658–660, Aug 1997.

[79] G. Durin and S. Zapperi. Scaling exponents for Barkhausen avalanches in polycrystalline and amorphous ferromagnets. *Physical review letters*, 84:4705–8, Jun 2000.

[80] S. Zapperi, P. Cizeau, G. Durin, and H. E. Stanley. Dynamics of a ferromagnetic domain wall: Avalanches, depinning transition, and the Barkhausen effect. *Phys. Rev. B*, 58:6353–6366, Sep 1998.

[81] T. Herranen and L. Laurson. Barkhausen noise from precessional domain wall motion. *Phys. Rev. Lett.*, 122:117205, Mar 2019.

[82] J. A. J. Burgess, A. E. Fraser, F. Fani Sani, D. Vick, B. D. Hauer, J. P. Davis, and M. R. Freeman. Quantitative magneto-mechanical detection and control of the barkhausen effect. *Science*, 339(6123):1051–1054, 2013.

[83] S. Papanikolaou, F. Bohn, R. L. Sommer, G. Durin, S. Zapperi, and J. P. Sethna. Universality beyond power laws and the average avalanche shape. *Nature Physics*, 7:316–320, Jan 2011.

[84] A. Benassi and S. Zapperi. Barkhausen instabilities from labyrinthine magnetic domains. *Phys. Rev. B*, 84:214441, Dec 2011.

[85] F. Bohn, G. Durin, M. Correa, N. Ribeiro Machado, R. Domingues Della Pace, C. Chesman, and R. Sommer. Playing with universality classes of Barkhausen avalanches. *Scientific Reports*, 8, Jan 2018.

[86] L. Laurson, G. Durin, and S. Zapperi. Universality classes and crossover scaling of Barkhausen noise in thin films. *Phys. Rev. B*, 89:104402, Mar 2014.

[87] V. M. Rudyak. The Barkhausen effect. *Soviet Physics Uspekhi*, 13(4):461–479, Apr 1971.

[88] J. C. McClure Jr. and K. Schroder. The magnetic Barkhausen effect. *C R C Critical Reviews in Solid State Sciences*, 6(1):45–83, 1976.

[89] O. Perković, K. Dahmen, and J. P. Sethna. Avalanches, Barkhausen noise, and plain old criticality. *Phys. Rev. Lett.*, 75:4528–4531, Dec 1995.

[90] G. Durin and S. Zapperi. The barkhausen effect. In *The Science of Hysteresis*, volume 2, pages 181 – 267. Apr 2004.

[91] B. Alessandro, C. Beatrice, G. Bertotti, and A. Montorsi. Domain wall dynamics and Barkhausen effect in metallic ferromagnetic materials. I. Theory. *Journal of Applied Physics*, 68(6):2901–2907, 1990.

[92] L. Thomas and S. Parkin. Current induced domain-wall motion in magnetic nanowires. In *Handbook of Magnetism and Advanced Magnetic Materials*. Wiley, 2007.

[93] R. Wieser, U. Nowak, and K. D. Usadel. Domain wall mobility in nanowires: Transverse versus vortex walls. *Phys. Rev. B*, 69:064401, Feb 2004.

[94] A. Kunz and B. Kastor. Micromagnetic simulations on the dependence of Gilbert damping on domain wall velocities in magnetic nanowires. In *2006 IEEE International Magnetics Conference (INTERMAG)*, pages 330–330, May 2006.

[95] R. Moriya, M. Hayashi, L. Thomas, C. Rettner, and S. Parkin. Dependence of field driven domain wall velocity on cross-sectional area in Ni65Fe20Co15 nanowires. *Applied Physics Letters*, 97(14):142506, 2010.

[96] N. L. Schryer and L. R. Walker. The motion of 180° domain walls in uniform dc magnetic fields. *Journal of Applied Physics*, 45(12):5406–5421, 1974.

[97] A. Mougin, M. Cormier, J. P. Adam, P. J. Metaxas, and J. Ferré. Domain wall mobility, stability and Walker breakdown in magnetic nanowires. *Europhysics Letters (EPL)*, 78(5):57007, May 2007.

[98] G. Beach, C. Nistor, C. Knutson, M. Tsoi, and J. Erskine. Dynamics of field-driven domain-wall propagation in ferromagnetic nanowires. *Nature materials*, 4:741–4, Nov 2005.

[99] Y. Nakatani, A. Thiaville, and J. E. Miltat. Faster magnetic walls in rough wires. *Nature materials*, 2 8:521–3, 2003.

[100] J. Lee, K. Lee, and S. Kim. Remarkable enhancement of domain-wall velocity in magnetic nanostripes. *Applied Physics Letters*, 91(12):122513, 2007.

[101] G Bertotti. Magnetic losses. In *Encyclopedia of Materials: Science and Technology*, pages 4798–4804. Dec 2001.

[102] J. E. L. Bishop. The influence of a random domain size distribution on the eddy-current contribution to hysteresis in transformer steel. *Journal of Physics D: Applied Physics*, 9(9):1367–1377, Jun 1976.

[103] S. Azzawi, A. T. Hindmarch, and D. Atkinson. Magnetic damping phenomena in ferromagnetic thin-films and multilayers. *Journal of Physics D: Applied Physics*, 50(47):473001, Oct 2017.

[104] R. D. McMichael and P. Krivosik. Classical model of extrinsic ferromagnetic resonance linewidth in ultrathin films. *IEEE Transactions on Magnetics*, 40(1):2–11, Jan 2004.

[105] L. Berger. Effect of interfaces on gilbert damping and ferromagnetic resonance linewidth in magnetic multilayers. *Journal of Applied Physics*, 90(9):4632–4638, 2001.

[106] Kh. Zakeri, J. Lindner, I. Barsukov, R. Meckenstock, M. Farle, U. von Hörsten, H. Wende, W. Keune, J. Rocker, S. S. Kalarickal, K. Lenz, W. Kuch, K. Baberschke, and Z. Frait. Spin dynamics in ferromagnets: Gilbert damping and two-magnon scattering. *Phys. Rev. B*, 76:104416, Sep 2007.

[107] H. J. Skadsem, Y. Tserkovnyak, A. Brataas, and G. E. W. Bauer. Magnetization damping in a local-density approximation. *Phys. Rev. B*, 75:094416, Mar 2007.

[108] Y. Tserkovnyak, A. Brataas, and G. E. W. Bauer. Spin pumping and magnetization dynamics in metallic multilayers. *Phys. Rev. B*, 66:224403, Dec 2002.

[109] D. L. Mills and S. M. Rezende. Spin damping in ultrathin magnetic films. In *Spin Dynamics in Confined Magnetic Structures II*, volume 87, pages 27–58. Feb 2003.

[110] M. Sparks. *Ferromagnetic-relaxation theory*. McGraw-Hill advanced physics monograph series. McGraw-Hill, 1964.

[111] R. D. McMichael and P. Krivosik. Classical model of extrinsic ferromagnetic resonance linewidth in ultrathin films. *IEEE Transactions on Magnetics*, 40(1):2–11, Jan 2004.

[112] K. Wu, M. Tang, D. Li, X. Guo, B. Cui, J. Yun, Y. Zuo, L. Xi, and Z. Z. Zhang. Modulation of magnetic damping constant of Fe2Co films by heavy doping of rare-earth Yb. *Journal of Physics D: Applied Physics*, 50(13):135001, Feb 2017.

[113] R. Urban, G. Woltersdorf, and B. Heinrich. Gilbert damping in single and multilayer ultrathin films: Role of interfaces in nonlocal spin dynamics. *Phys. Rev. Lett.*, 87:217204, Nov 2001.

[114] C. Fusco, D. E. Wolf, and U. Nowak. Magnetic friction of a nanometer-sized tip scanning a magnetic surface: Dynamics of a classical spin system with direct exchange and dipolar interactions between the spins. *Phys. Rev. B*, 77:174426, May 2008.

[115] M. P. Magiera, D. E. Wolf, L. Brendel, and U. Nowak. Magnetic friction and the role of temperature. *IEEE Transactions on Magnetics*, 45(10):3938–3941, Oct 2009.

[116] M. P. Magiera, S. Angst, A. Hucht, and D. E. Wolf. Magnetic friction: From Stokes to Coulomb behavior. *Phys. Rev. B*, 84:212301, Dec 2011.

[117] D. Kadau, A. Hucht, and D. E. Wolf. Magnetic friction in Ising spin systems. *Phys. Rev. Lett.*, 101:137205, Sep 2008.

[118] A. Benassi. Dynamics of mobile interacting ferromagnetic films: theory and numerical implementation. *Modelling and Simulation in Materials Science and Engineering*, 22(2):025004, Jan 2014.

[119] A. Benassi, J. Schwenk, M. A. Marioni, H. J. Hug, and D. Passerone. Microscale motion control through ferromagnetic films. *Advanced Materials Interfaces*, 1(4):1400023, 2014.

[120] B. C. Stipe, H. J. Mamin, T. D. Stowe, T. W. Kenny, and D. Rugar. Magnetic dissipation and fluctuations in individual nanomagnets measured by ultrasensitive cantilever magnetometry. *Phys. Rev. Lett.*, 86:2874–2877, Mar 2001.

[121] L. D. Landau and E. Lifshitz. On the theory of the dispersion of magnetic permeability in ferromagnetic bodies. *Phys. Z. Sowjet.*, 8:153, 1935.

[122] N. S. Akulov. Zur theorie der magnetisierungskurve von einkristallen. *Zeitschrift für Physik*, 67(11):794–807, Nov 1931.

[123] W.F. Brown. *Micromagnetics*. Interscience tracts on physics and astronomy. Interscience Publishers, 1963.

[124] H. Kronmüller. General micromagnetic theory. In *Handbook of Magnetism and Advanced Magnetic Materials*. Wiley, 2007.

[125] J. E. Miltat and M. J. Donahue. Numerical micromagnetics: Finite difference methods. In *Handbook of Magnetism and Advanced Magnetic Materials*. John Wiley & Sons, Ltd, 2007.

[126] M. d'Aquino. *Nonlinear Magnetization Dynamics in Thin-Films and Nanoparticles*. PhD thesis, Jun 2019.

[127] T. Schrefl, H. Forster, D. Suess, W. Scholz, V. D. Tsiantos, and J. Fidler. Micromagnetic simulation of switching events. In *Advances in Solid State Physics*, volume 41, pages 623–635. Jul 2001.

[128] S. Jung, J. B. Ketterson, and V. Chandrasekhar. Micromagnetic calculations of ferromagnetic resonance in submicron ferromagnetic particles. *Phys. Rev. B*, 66:132405, Oct 2002.

[129] F. Bloch. Zur theorie des austauschproblems und der remanenzerscheinung der ferromagnetika. *Zeitschrift für Physik*, 74(5):295–335, May 1932.

[130] T. L. Gilbert. A Lagrangian formulation of the gyromagnetic equation of the magnetization field. *Phys. Rev.*, 100:1243, 1955.

[131] C. Papusoi, T. Le, C. C. H. Lo, C. Kaiser, M. Desai, and R. Acharya. Measurements of gilbert damping parameter α for CoPt-based and CoFe-based films for magnetic recording applications. *Journal of Physics D: Applied Physics*, 51(32):325002, Jul 2018.

[132] W. F. Brown. Thermal fluctuations of a single-domain particle. *Journal of Applied Physics*, 34(4):1319–1320, 1963.

[133] S. Zhang and Z. Li. Roles of nonequilibrium conduction electrons on the magnetization dynamics of ferromagnets. *Phys. Rev. Lett.*, 93:127204, Sep 2004.

[134] A. N. Bogdanov and U. K. Rößler. Chiral symmetry breaking in magnetic thin films and multilayers. *Phys. Rev. Lett.*, 87:037203, Jun 2001.

[135] A. E. LaBonte. Two-dimensional Bloch-type domain walls in ferromagnetic films. *Journal of Applied Physics*, 40:2450–2458, May 1969.

[136] R. Hertel, O. Fruchart, S. Cherifi, P. O. Jubert, S. Heun, A. Locatelli, and J. Kirschner. Three-dimensional magnetic flux-closure patterns in mesoscopic Fe islands. *Physical Review B : Condensed matter and materials physics*, 72:214409, 2005.

[137] O. N. Martyanov, V. F. Yudanov, R. N. Lee, S. A. Nepijko, H. J. Elmers, R. Hertel, C. M. Schneider, and G. Schönhense. Ferromagnetic resonance study of thin film antidot arrays: Experiment and micromagnetic simulations. *Physical Review B*, 75(17):174429, May 2007.

[138] Thiaville, A., Miltat, J., and Ben Youssef, J. Dynamics of vertical bloch lines in bubble garnets: Experiments and theory. *Eur. Phys. J. B*, 23(1):37–47, 2001.

[139] L. Lopez-Diaz, D. Aurelio, L. Torres, E. Martinez, M. A. Hernandez-Lopez, J. Gomez, O. Alejos, M. Carpentieri, G. Finocchio, and G. Consolo. Micromagnetic simulations using graphics processing units. *Journal of Physics D: Applied Physics*, 45(32):323001, 2012.

[140] A. Vansteenkiste and B. Van de Wiele. Mumax: A new high-performance micromagnetic simulation tool. *Journal of Magnetism and Magnetic Materials*, 323(21):2585 – 2591, 2011.

[141] J. Fidler and T. Schrefl. Micromagnetic modelling - the current state of the art. *Journal of Physics D: Applied Physics*, 33(15):R135–R156, Jul 2000.

[142] A. Vansteenkiste, J. Leliaert, M. Dvornik, M. Helsen, F. Garcia-Sanchez, and B. Van Waeyenberge. The design and verification of mumax3. *AIP Adv.*, 4(10):107133, 2014.

[143] G. S. Abo, Y. Hong, J. Park, J. Lee, W. Lee, and B. Choi. Definition of magnetic exchange length. *IEEE Transactions on Magnetics*, 49(8):4937–4939, Aug 2013.

[144] D. V. Berkov, K. Ramstöcck, and A. Hubert. Solving micromagnetic problems. Towards an optimal numerical method. *physica status solidi (a)*, 137(1):207–225, 1993.

[145] J. A. Fernandez-Roldan, D. Serantes, R. P. del Real, M. Vazquez, and O. Chubykalo-Fesenko. Micromagnetic evaluation of the dissipated heat in cylindrical magnetic nanowires. *Applied Physics Letters*, 112(21):212402, 2018.

[146] M. Madami, M. d'Aquino, G. Gubbiotti, S. Tacchi, C. Serpico, and G. Carlotti. Micromagnetic study of minimum-energy dissipation during landauer erasure of either isolated or coupled nanomagnetic switches. *Phys. Rev. B*, 90:104405, Sep 2014.

[147] G. Csaba, P. Lugli, and W. Porod. Power dissipation in nanomagnetic logic devices. In *4th IEEE Conference on Nanotechnology, 2004.*, pages 346–348, Aug 2004.

[148] S. Russek, R. McMichael, M. Donahue, and S. Kaka. High speed switching and rotational dynamics in small magnetic thin film devices. In *Topics in applied physics*, volume 87, pages 93–156. Feb 2003.

[149] D. V. Berkov. Magnetization dynamics including thermal fluctuations: Basic phenomenology, fast remagnetization processes and transitions over high-energy barriers. In *Handbook of Magnetism and Advanced Magnetic Materials*. Wiley, 2007.

[150] T. L. Gilbert. A phenomenological theory of damping in ferromagnetic materials. *IEEE Transactions on Magnetics*, 40(6):3443–3449, Nov 2004.

Aalto-DD 161/2019

ISBN 978-952-60-8705-4 (printed)
ISBN 978-952-60-8706-1 (pdf)
ISSN 1799-4934 (printed)
ISSN 1799-4942 (pdf)

Aalto University
School of Science
Department of Applied Physics
www.aalto.fi

BUSINESS + ECONOMY

ART + DESIGN + ARCHITECTURE

SCIENCE + TECHNOLOGY

CROSSOVER

DOCTORAL DISSERTATIONS